

# Understanding the Reversal Curse Mitigation in Masked Diffusion Models through Attention and Training Dynamics

Sangwoo Shin <sup>\*1</sup> BumJun Kim <sup>\*1</sup> Kyelim Lee <sup>\*1</sup> Moongyu Jeon <sup>\*1</sup> Albert No <sup>1</sup>

## Abstract

Autoregressive language models (ARMs) suffer from the reversal curse: after learning “*A* is *B*,” they often fail on the reverse query “*B* is *A*.” Masked diffusion-based language models (MDMs) exhibit this failure in a much weaker form, but the underlying reason has remained unclear. A common explanation attributes this mitigation to the any-order training objective. However, observing “[M] is *B*” during training does not necessarily teach the model to handle the reverse prompt “*B* is [M].” We show that the mitigation arises from architectural structure and its interaction with training. In a one-layer Transformer encoder, weight sharing couples the two directions by making forward and reverse attention scores positively correlated. In the same setting, we further show that the corresponding gradients are aligned, so minimizing the forward loss also reduces the reverse loss. Experiments on both controlled toy tasks and large-scale diffusion language models support these mechanisms, explaining why MDMs partially overcome a failure mode that persists in strong ARMs.

## 1. Introduction

Since the advent of the Transformer architecture (Vaswani et al., 2017), language models have advanced rapidly (Devlin et al., 2019; Raffel et al., 2020). Transformer decoder-based Autoregressive Models (ARMs) (Radford et al., 2018; 2019; Brown et al., 2020) have become the dominant paradigm for large language models (LLMs) (Grattafiori et al., 2024; OpenAI, 2023). Despite their success, ARMs exhibit structural limitations. A notable example is the *reversal curse* (Berglund et al., 2024): after learning the fact “*A* is *B*”, they often fail to answer the logically equivalent reverse query “*B* is *A*”. This arises because ARMs are op-

timized only for the unidirectional conditional probability  $p(y = B|x = A)$ , without explicitly modeling the reverse probability  $p(y = A|x = B)$ . For instance, a model may correctly predict “The capital of France is Paris,” yet fail to answer “Which country has Paris as its capital?” Data augmentation (Golovneva et al., 2024; Lu et al., 2024; Lv et al., 2024; Zhang et al., 2025) can partially alleviate the problem, but they do not resolve the bias fundamentally.

Masked diffusion-based language models (MDMs) (Austin et al., 2021; Campbell et al., 2022; Lou et al., 2024; Sahoo et al., 2024; Shi et al., 2024; Ou et al., 2025), implemented with Transformer encoders and trained via random masking and reconstruction, have recently emerged as a promising alternative to ARMs. They offer several advantages: the encoder architecture naturally supports bidirectional context modeling, the random masking objective enables generation in any-order, and recent work has demonstrated their scalability to the LLM regime (Nie et al., 2025b; Ye et al., 2025). In addition, MDMs have been reported to handle reverse queries more effectively than ARMs (Kitouni et al., 2024; Nie et al., 2025a;b), suggesting a potential structural advantage. However, these observations remain anecdotal, and no systematic analysis has yet been provided.

We begin by establishing, through systematic experiments on large-scale language models, that MDMs mitigate the reversal curse. While prior work explored this phenomenon at the 1.1B scale (Nie et al., 2025a) and LLaDA (Nie et al., 2025b) demonstrated preliminary capabilities on poem completion tasks, we advance this analysis by conducting controlled evaluations on knowledge-retrieval benchmarks at the 7-8B scale. Comparing ARMs (LLaMA-3.1 (Grattafiori et al., 2024), Qwen-2.5 (Yang et al., 2025)) with an MDM (LLaDA (Nie et al., 2025b)) across benchmarks such as Parent-Child and Person-Description, we find that MDMs consistently succeed on reverse inference tasks where strong ARMs collapse. These large-scale results provide systematic evidence that the reversal curse is substantially alleviated in MDMs under realistic evaluation settings.

Having established the phenomenon, we then ask: *why do MDMs succeed on reversal tasks where ARMs fail?* A common intuition points to the any-order nature of the MDM training objective: random masking provides supervision

<sup>\*</sup>Equal contribution <sup>1</sup>Department of Artificial Intelligence, Yonsei University, Seoul, Republic of Korea. Correspondence to: Albert No <albertno@yonsei.ac.kr>.

across all conditional directions. Yet, this explanation is incomplete. By formulation, the probability of unmasking  $[\mathbf{M}]$  as  $A$  in “[ $\mathbf{M}$ ] is  $B$ ” corresponds to  $p(x=A|y=B)$ , whereas the reverse query “ $B$  is [ $\mathbf{M}$ ]” requires  $p(y=A|x=B)$  as described in Figure 1. These two conditional probabilities are defined with respect to different conditioning events, and the training objective provides no mechanism to establish a systematic relation between them.

We demonstrate that the key to reversal ability lies in the Transformer encoder architecture of MDMs. In a simplified one-layer setting, we identify an architectural coupling between conditionals that are otherwise unrelated: the attention strengthened by forward training is positively correlated with the attention required for reverse inference. Beyond this static mechanism, we further characterize training dynamics by proving that the gradients of the forward and reverse objectives are aligned, so optimizing the forward loss also reduces the reverse loss. We validate both predictions, attention-score correlation and gradient alignment, in controlled toy experiments and large-scale settings.

In summary, our contributions are:

- **Large-scale experiments:** We systematically evaluate 7–8B parameter models and show that MDMs consistently outperform ARMs on reversal tasks.
- **Theoretical insight:** We show that the reversal capability of MDMs stems from architectural structure in the Transformer encoder and its coupling with optimization dynamics during training.
- **Empirical validation:** Synthetic toy experiments and large-scale diffusion LLMs confirm the theoretical predictions and show consistent alignment across scales.

## 2. Preliminaries

### 2.1. Autoregressive Models vs. Masked Diffusion Models

In this section, we review autoregressive models (ARMs) and masked diffusion models (MDMs) with a focus on their training objectives and architectures. Within the architecture, our analysis centers on the self-attention mechanism of the Transformer encoder used in MDMs, which governs how models process context and is crucial for understanding their capacity for reverse inference.

**Training Objectives.** An ARM (Radford et al., 2018; 2019) is trained to generate a sequence  $\mathbf{x} = x_1 x_2 \dots x_L$  strictly in a left-to-right manner. Given a prefix  $\mathbf{x}_{<i} = x_1 x_2 \dots x_{i-1}$ , the model maximizes the conditional probability of the next token  $x_i$ . Formally, the training objective

is the following cross-entropy loss:

$$\mathcal{L}_{\text{ARM}}(\mathbf{x}; \theta) = - \sum_{i=1}^L \log p_{\theta}(x_i | \mathbf{x}_{<i}).$$

By contrast, an MDM (Sahoo et al., 2024; Shi et al., 2024; Ou et al., 2025) learns to generate a sequence in an any-order fashion via random masking. Let  $\mathbf{x}^t$  denote a corrupted version of  $\mathbf{x}$  in which each token is independently replaced by the special mask token  $[\mathbf{M}]$  with probability  $t \in [0, 1]$ . The model is then trained to recover the original tokens at the masked positions by maximizing the conditional probability of each masked token. The formal training objective is the following weighted cross-entropy loss:

$$\mathcal{L}_{\text{MDM}}(\mathbf{x}; \theta) = -\mathbb{E}_{t \sim \mathcal{U}[0,1], \mathbf{x}^t} \left[ \frac{1}{t} \sum_{i: x_i^t = [\mathbf{M}]} \log p_{\theta}(x_i | \mathbf{x}^t) \right].$$

**Architectures.** An ARM models  $p_{\theta}(x_i | \mathbf{x}_{<i})$  with a Transformer decoder that uses causal attention. At each step  $i$ , the decoder takes the prefix  $\mathbf{x}_{<i}$  as input and produces a probability distribution over the vocabulary  $\mathcal{V}$ , from which the next token  $x_i$  is drawn.

In contrast, an MDM models  $p_{\theta}(x_i | \mathbf{x}^t)$  with a Transformer encoder that applies full-attention. The encoder processes the corrupted sequence  $\mathbf{x}^t$ , which contains  $[\mathbf{M}]$  at a subset of positions, and produces a distribution over  $\mathcal{V}$  at every position  $i$ . The outputs at masked positions specify the probabilities of reconstructing the masked tokens.

**Self-Attention in the Transformer Encoder.** Since our theory centers on how MDMs route information through a Transformer encoder, we briefly define self-attention in the single-head case with head dimension  $D$ . Given token embeddings  $\mathbf{h}_i \in \mathbb{R}^D$ , the encoder uses shared linear projections  $\mathbf{W}_Q, \mathbf{W}_K, \mathbf{W}_V \in \mathbb{R}^{D \times D}$  to form

$$\mathbf{q}_i = \mathbf{W}_Q \mathbf{h}_i, \quad \mathbf{k}_i = \mathbf{W}_K \mathbf{h}_i, \quad \mathbf{v}_i = \mathbf{W}_V \mathbf{h}_i.$$

For a query at position  $i$  and a key at position  $j$ , the (RoPE) attention score is

$$S_{ij} = \mathbf{q}_i^\top \mathbf{R}(j-i) \mathbf{k}_j,$$

where  $\mathbf{R}(\Delta)$  is the RoPE rotation matrix for relative offset  $\Delta$  (Su et al., 2024). The scores are scaled and normalized to obtain attention weights

$$\alpha_{ij} = \frac{\exp\left(\frac{1}{\sqrt{D}} S_{ij}\right)}{\sum_{j'=1}^L \exp\left(\frac{1}{\sqrt{D}} S_{ij'}\right)}.$$

Finally, the context vector at position  $i$  is the weighted sum of value vectors:

$$\mathbf{c}_i = \sum_{j=1}^L \alpha_{ij} \mathbf{v}_j.$$

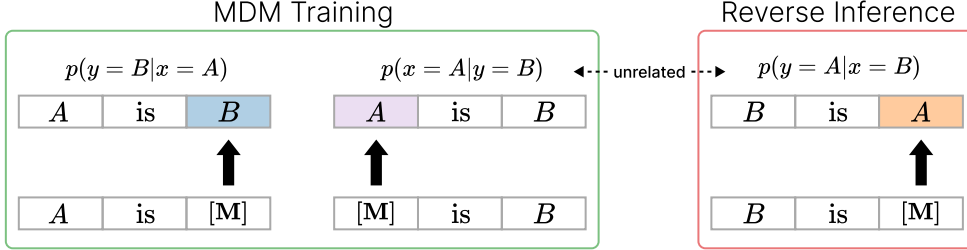


**Figure 1. Why the training objective of MDMs does not directly enable reverse inference.** When  $A$  is masked in “ $A$  is  $B$ ,” the model only learns to restore  $A$  from “[M] is  $B$ ,” i.e.,  $p(x = A|y = B)$ . True reversal instead requires  $p(y = A|x = B)$ , restoring  $A$  from “ $B$  is [M],” which is mathematically unrelated to  $p(x = A|y = B)$  under the MDM objective. Thus, training with random masking cannot by itself explain reversal capability; additional architectural factors must account for the observed success.

Thus, the attention weight  $\alpha_{ij}$  determines how strongly token  $i$  draws information from token  $j$ ; in particular, when predicting a masked token, the weight from [M] to an informative token (e.g.,  $B$ ) governs how the model uses context to reconstruct the target.

## 2.2. The Reversal Curse in Autoregressive Models

As discussed in Section 2.1, autoregressive models (ARMs) generate text in a strictly left-to-right manner. This design leads to the well-documented *reversal curse* (Berglund et al., 2024): even after learning a relation expressed in the forward direction, models often fail to answer the corresponding reversed query. Following the seminal formulation in Berglund et al. (2024), we use the shorthand notation “ $A$  is  $B$ ” versus “ $B$  is  $A$ ” to denote a forward fact and its reversed query. Note that the underlying relation is not restricted to the literal verb *is*. For example, a model may learn “The capital of France is Paris,” yet fail to answer the reversed form “Which country has Paris as its capital?”

Several data-centric approaches have been explored to alleviate the reversal curse in ARMs, including analyses that attribute the failure to training-data structure and biases, as well as augmentation-based strategies that inject (partially) reversed variants and controlled studies that isolate contributing factors (Lin et al., 2024; Golovneva et al., 2024; Lu et al., 2024).

While these interventions can reduce the gap in specific settings, they do not fundamentally address the objective-level asymmetry of left-to-right next-token prediction. Concretely, an ARM learns the relation “ $A$  is  $B$ ” by maximizing only the forward conditional probability  $p_\theta(y = !B|x = !A)$ . This training objective is entirely decoupled from the reverse conditional  $p_\theta(y = A|x = B)$ , making reverse inference an independent task rather than a byproduct of forward learning. This limitation is not just intuitive but also formal: a gradient-based analysis of a one-layer Transformer decoder shows that optimizing  $p_\theta(y = B|x = A)$  provides essentially no learning signal for improving  $p_\theta(y = A|x = B)$  (Zhu et al., 2024). Motivated by this perspective on the interplay

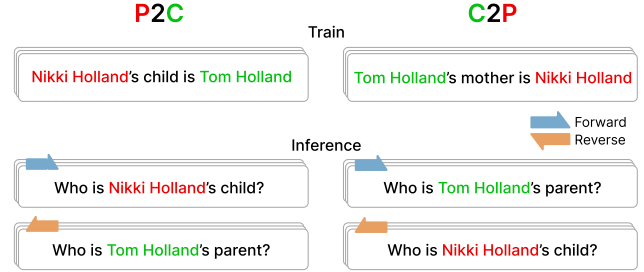


**Figure 2. Illustration of the evaluation setup on the Parent-Child task.** Each model is trained only in forward direction (e.g., parent → child or child → parent) and then evaluated on both forward and reverse queries. Forward queries follow the trained mapping and reverse queries require the unseen inverse mapping.

between training dynamics and model architecture, we analyze how the Transformer architecture of MDMs, when coupled with gradient-based training, can propagate learning signals across different conditioning directions.

## 3. Large-Scale Systematic Experiments

As discussed in Section 2.2, autoregressive next-token prediction optimizes a unidirectional conditional, which prevents ARMs from answering reversal queries. By contrast, MDMs receive bidirectional supervision via random masking and have been reported to alleviate the reversal curse (Kitouni et al., 2024; Nie et al., 2025a,b). We provide a large-scale systematic comparison of ARMs and MDMs on reverse inference.

**Setup.** Training data consists only of *forward* relational statements. For example, in the P2C type Parent-Child task, the model is trained on sentences such as “Nikki Holland’s child is Tom Holland,” while the reversed form “Tom Holland’s parent is Nikki Holland” is never observed during training. In our earlier abstract formulation, these correspond to forward statements of the form “ $A$  is  $B$ ” and their reversed counterparts “ $B$  is  $A$ ,” respectively. At evaluation, we test both directions by constructing forward and reverse queries from the entity pair.

Table 1. Results of Parent–Child, Person–Description and T-REx datasets for large-scale evaluation. **Across all cases, LLaDA (MDM) shows notably strong performance in reverse inference accuracy.** In contrast, LLaMA-3.1 and Qwen-2.5 (ARMs) nearly collapse to random guessing and almost completely fail to perform reverse inference. Results are averaged across 3 random seeds.

Train Dataset	MDM		ARM			
	LLaDA 8B		LLaMA-3.1 8B		Qwen-2.5 7B	
	Forward	Reverse	Forward	Reverse	Forward	Reverse
Parent → Child (P2C)	76.7	<b>48.3</b>	89.9	15.9	89.9	0.5
Child → Parent (C2P)	87.7	<b>43.7</b>	95.9	6.9	89.0	1.4
Person → Description (P2D)	72.7	<b>99.5</b>	72.7	3.5	70.7	2.2
Description → Person (D2P)	99.7	<b>41.3</b>	83.0	1.8	80.0	1.5
T-REx	92.3	<b>81.5</b>	87.3	2.8	89.8	2.3

We use three large-scale tasks adapted from [Berglund et al. \(2024\)](#) and [Elsahar et al. \(2018\)](#): *Parent–Child*, *Person–Description*, and *T-REx*. For all tasks, we train *only* on forward pairs and exclude any reversed pairs. Each dataset is constructed to yield *unambiguous* mappings between entities (one input maps to a single target under the chosen relation), so that exact-match evaluation is well defined. For T-REx, we select six (near-)functional relations from the original knowledge base triplets and filter to retain unique head-tail mappings; we additionally convert each entity into a *virtual name* to reduce reliance on memorized world knowledge and to ensure the mapping must be learned from fine-tuning. Forward queries follow the training direction, while reverse queries swap the input and output roles. Figure 2 illustrates representative forward/reverse examples. We report exact-match accuracy after minimal normalization (e.g., stripping whitespace and case-folding), with further dataset details in Appendix C.

**Models.** We evaluate three large-scale LLMs. LLaDA 8B Instruct ([Nie et al., 2025b](#)) is an MDM that uses a Transformer encoder and iterative denoising-style generation, and targets LLaMA-3 as its primary comparison. For ARMs, we include LLaMA-3.1 8B Instruct ([Grattafiori et al., 2024](#)) and Qwen-2.5 7B Instruct ([Yang et al., 2025](#)). All models are fine-tuned on the *same* forward-only training instances using LoRA ([Hu et al., 2022](#)) (Appendix C for hyperparameters), and we use deterministic decoding for all evaluations to ensure a consistent comparison.

**Results.** Table 1 reports accuracy on Parent–Child, Person–Description, and T-REx. All models achieve strong performance in the *Forward* regime, confirming they can fit the observed forward mappings. In the *Reverse* regime, however, LLaMA-3.1 and Qwen-2.5 drop sharply, often to near-random levels, exhibiting the autoregressive reversal curse described in Section 2.2. In contrast, LLaDA maintains consistently high reverse accuracy across all three tasks, despite never seeing reversed pairs during training.

These results show that the reversal mitigation in MDMs extends beyond simple templates to diverse relational settings, whereas it remains largely absent in ARMs.

## 4. Theoretical Analysis

### 4.1. Incompleteness of Objective-Only Explanation

In Section 3, we observed that MDMs mitigate the reversal curse substantially more than ARMs. A common intuition attributes this to any-order supervision from random masking ([Kitouni et al., 2024](#); [Nie et al., 2025a,b](#)). However, for a training instance “*A* is *B*,” the objective supervises conditionals such as  $p_\theta(y = B|x = A)$  (from “*A* is [M]”) and  $p_\theta(x = A|y = B)$  (from “[M] is *B*”), but it does not directly supervise the reverse-query conditional  $p_\theta(y = A|x = B)$  required by “*B* is [M]” (see Figure 1).

Consequently, the effective mitigation of the reversal curse observed in practice (Section 3) cannot be attributed solely to the training objective. Instead, we argue that a plausible explanation emerges only when the *architectural properties* of the Transformer are considered. In the following subsections, we dissect the interplay between this architecture and the training dynamics through a two-fold theoretical framework: we first examine the structural inductive bias inherent in the architecture (Section 4.2), and subsequently analyze the training dynamics on this architecture (Section 4.3).

### 4.2. Structural Coupling of Attention

In this subsection, we study a *structural inductive bias* of the Transformer encoder used in MDMs. We show that the RoPE-equipped full-attention architecture induces a statistical coupling between the attention score reinforced by forward training (**forward attention**) and the attention score required for reversal (**reverse attention**). In particular, the two scores are positively correlated, so strengthening the forward attention pathway tends to strengthen the reverse pathway as well.

Following the simplified but mechanistically transparent setup of Zhu et al. (2024), we analyze a single-layer Transformer encoder with RoPE. In this setting, the attention score  $\mathbf{q}_{[\mathbf{M}]}^\top \mathbf{R}(\Delta) \mathbf{k}$  determines how strongly the mask query  $\mathbf{q}_{[\mathbf{M}]}$  attends to a context key  $\mathbf{k}$  at relative distance  $\Delta$ . If reversal succeeds, the model must still identify the informative token  $B$  under swapped order, suggesting that a built-in coupling between forward and reverse attention scores can serve as a mechanism for reversal.

Consider the forward prompt “[M] is  $B$ ” and the reverse prompt “ $B$  is [M]”. Let  $\Delta_1$  and  $\Delta_2$  denote the relative distances between [M] and  $B$  in the two prompts. We define the forward attention score reinforced during training and the reverse attention score required at test time as

$$S_{\text{fwd}} = \mathbf{q}_{[\mathbf{M}]}^\top \mathbf{R}(\Delta_1) \mathbf{k}_B, \quad S_{\text{rev}} = \mathbf{q}_{[\mathbf{M}]}^\top \mathbf{R}(-\Delta_2) \mathbf{k}_B.$$

Although the relative positions differ, the key question is whether these scores *co-vary*. Intuitively, if training increases the alignment between  $\mathbf{q}_{[\mathbf{M}]}$  and  $\mathbf{k}_B$  to raise  $S_{\text{fwd}}$ , the rotational structure of RoPE suggests that  $S_{\text{rev}}$  should often increase as well.

To formalize the effect above while keeping the analysis tractable, we make the following assumptions. To capture the learned alignment characteristic of a trained model, we explicitly model the conditional dependence  $\mathbf{k}|\mathbf{q}$  through a RoPE-consistent second-moment structure.

- **(A1) Query distribution.**  $\mathbf{q} \sim \mathcal{N}(\mathbf{0}, \sigma^2 \mathbf{I}_D)$ .
- **(A2) RoPE-consistent learned alignment.** The conditional covariance  $\Sigma(\mathbf{q}) = \text{Cov}(\mathbf{k}|\mathbf{q})$  is block-diagonal with  $2 \times 2$  blocks  $\Sigma_i$ , and within each RoPE plane we have  $\Sigma_i \mathbf{q}_i = \lambda_i \mathbf{q}_i$  for all  $i$ .
- **(A3) Symmetric distances.**  $\Delta_1 = \Delta_2 = \Delta$ .

Assumption (A1) models the query  $\mathbf{q}$  as an isotropic Gaussian. Since we encapsulate the entire learned dependency structure between queries and keys within the conditional distribution  $\mathbf{k}|\mathbf{q}$  in Assumption (A2), we simply treat the marginal distribution of  $\mathbf{q}$  as random. Assumption (A2) encodes the *minimal* structure we need from learning: keys become statistically more aligned with queries *within each RoPE 2D subspace*, while respecting RoPE’s rotational decomposition. Concretely, the block-diagonal form matches RoPE’s  $2 \times 2$  rotation planes, and the eigenvector condition formalizes that, in each plane, the direction of  $\mathbf{q}_i$  is a principal direction of variability for  $\mathbf{k}_i$  given  $\mathbf{q}$ , thereby capturing the essential geometric alignment through the covariance structure. Assumption (A3) is adopted for clarity and matches the canonical two-entity template where the informative token lies at the same absolute distance in the forward and reverse prompts.

**Theorem 4.1.** *Under (A1)–(A3), the expected correlation between the forward and reverse attention scores satisfies*

$$\mathbb{E}_{\mathbf{q}} \left[ \text{Corr} \left( \mathbf{q}^\top \mathbf{R}(\Delta) \mathbf{k}, \mathbf{q}^\top \mathbf{R}(-\Delta) \mathbf{k} \mid \mathbf{q} \right) \right] \geq \frac{1}{D} \text{Tr}(\mathbf{R}(2\Delta)).$$

For typical relative positions (e.g.,  $\Delta \leq 50$ ), the right-hand side admits the approximation

$$\frac{1}{D} \text{Tr}(\mathbf{R}(2\Delta)) \gtrsim \frac{\log 100 - \gamma - 2/100}{\log 10000} \approx 0.435, \quad (1)$$

where  $\gamma \approx 0.577$  is the Euler–Mascheroni constant. See Section A for the proof of Theorem 4.1, the derivation of Equation (1), and a stronger Cantelli-type tail bound.

Theorem 4.1 formalizes a structural inductive bias: forward and reverse attention scores are expected to be positively correlated. Concretely, when training on “[M] is  $B$ ” encourages the model to attend to the informative token  $B$  (Clark et al., 2019; Zucchet et al., 2025) and thereby increase  $S_{\text{fwd}}$ , the RoPE-equipped encoder architecture statistically encourages a corresponding increase in  $S_{\text{rev}}$  for “ $B$  is [M]” as well. In Sections 5.1 and 6.1, we empirically verify that this coupling holds in practice:  $S_{\text{rev}}$  rises in tandem with  $S_{\text{fwd}}$  in both controlled toy settings and large-scale diffusion LLMs.

### 4.3. Transfer via Gradient Alignment

The previous subsection established a *static* coupling: in a RoPE-equipped encoder, forward and reverse attention scores are positively correlated. We now show a complementary *dynamic* coupling: in the same simplified setting, optimizing the forward objective produces parameter updates that also reduce the reverse loss.

**Setup.** We consider the minimal case where the input contains a single mask token and a single informative context token  $B$ , but allow their relative offsets to vary (to reflect that the pair may appear at different positions inside a longer sequence). Let

$$\begin{aligned} \mathbf{x}_{\text{fwd}} &= ([\mathbf{M}], B) \text{ with relative distance } \Delta_1 > 0, \\ \mathbf{x}_{\text{rev}} &= (B, [\mathbf{M}]) \text{ with relative distance } \Delta_2 > 0 \end{aligned}$$

and define the masked-token cross-entropy losses

$$\begin{aligned} \mathcal{L}_{\text{fwd}}(\theta) &= -\log p_\theta([\mathbf{M}] = A \mid \mathbf{x}_{\text{fwd}}), \\ \mathcal{L}_{\text{rev}}(\theta) &= -\log p_\theta([\mathbf{M}] = A \mid \mathbf{x}_{\text{rev}}). \end{aligned}$$

In the notation of the previous sections, these losses are defined from  $p_\theta(x = A \mid y = B)$  and  $p_\theta(y = A \mid x = B)$  while ignoring the effects of other tokens for analytical clarity.

Let  $\mathbf{g}_{\text{fwd}} = \nabla_\theta \mathcal{L}_{\text{fwd}}(\theta)$  and  $\mathbf{g}_{\text{rev}} = \nabla_\theta \mathcal{L}_{\text{rev}}(\theta)$ . Consider one gradient step on the forward loss,  $\theta^+ = \theta - \eta \mathbf{g}_{\text{fwd}}$ . For sufficiently small  $\eta$ , a first-order expansion gives

$$\mathcal{L}_{\text{rev}}(\theta^+) - \mathcal{L}_{\text{rev}}(\theta) \approx -\eta \langle \mathbf{g}_{\text{rev}}, \mathbf{g}_{\text{fwd}} \rangle.$$

Thus, if  $\langle \mathbf{g}_{\text{rev}}, \mathbf{g}_{\text{fwd}} \rangle > 0$ , then forward training *constructively decreases* the reverse loss to first order.

We analyze a single-layer, single-head Transformer encoder with fixed embeddings, trainable parameters ( $\mathbf{W}_Q, \mathbf{W}_K, \mathbf{W}_V, \mathbf{W}_O$ ), and RoPE, in a form compatible with the setup in Section 4.2. In this model, the forward-reverse gradient inner product admits an explicit decomposition across parameter blocks. Crucially, the query/key contributions contain the same RoPE-induced geometric factor that appeared in the attention-correlation analysis, namely a quadratic form of  $\mathbf{R}(\Delta_1 + \Delta_2)$ . This yields the following implication:

**Theorem 4.2** (Forward-to-reverse transfer via gradient alignment). *In the one-layer Transformer encoder described above, under mild non-saturation and consistency conditions (stated in Appendix B), the forward and reverse gradients are positively aligned:*

$$\langle \mathbf{g}_{\text{rev}}, \mathbf{g}_{\text{fwd}} \rangle > 0.$$

Consequently, a forward gradient step decreases the reverse loss to first order, i.e.,  $\mathcal{L}_{\text{rev}}(\theta - \eta \mathbf{g}_{\text{fwd}}) < \mathcal{L}_{\text{rev}}(\theta)$  for sufficiently small  $\eta$ .

**Interpretation.** The takeaway is that the same architectural ingredients that couple forward and reverse *attention* also couple forward and reverse *optimization*. Because the encoder shares attention parameters across positions and RoPE ties together relative offsets through  $\mathbf{R}(\Delta_1 + \Delta_2)$ , learning signals from the forward configuration can directly move parameters in a direction that improves the reverse configuration, even though the reverse conditional is not explicitly supervised.

Appendix B provides the full decomposition, assumptions, and proof. Empirically, we observe positive alignment throughout training in our toy setting and in large-scale diffusion LLMs (see Sections 5.2 and 6.2).

## 5. Toy-Scale Validation

To verify our theoretical analysis, we design controlled toy experiments to examine whether reverse inference emerges in practice and whether the attention mechanism behaves as predicted. We compare a one-layer ARM (GPT-2 (Radford et al., 2019)) with a one-layer MDM (RADD (Ou et al., 2025)) as RADD is implemented to target GPT-2.

**Experimental Setup** We construct a synthetic dataset where each sequence of length  $L$  contains exactly one lowercase–uppercase pair and the remaining positions are padded with zeros. This instantiates our “ $A$  is  $B$ ” template, where  $A$  is the lowercase token and  $B$  is its uppercase counterpart. During training, we enforce the forward ordering:

Table 2. Accuracy (%) of the toy experiment, averaged over 3 random seeds. Only MDM exhibits reversal capability.

Length	MDM		ARM	
	Forward	Reverse	Forward	Reverse
$L = 10$	99.31	<b>43.10</b>	99.83	0.00
$L = 20$	97.36	<b>55.70</b>	99.80	0.00
$L = 30$	96.91	<b>33.89</b>	99.93	0.00
$L = 40$	97.27	<b>38.37</b>	99.93	0.00

the lowercase letter always appears before its corresponding uppercase, and we exclude any sequence with the reversed order. For example, with  $L = 3$  and the pair (d, D), valid training instances include dD0, d0D, and 0dD, whereas reversed forms Dd0, D0d, and 0Dd never appear.

At test time, we probe both directions using a prefix prompt. For the forward test, we prompt the model with d at the first position and check whether it generates the corresponding D *at any position* in the length- $L$  output. For the reverse test, we prompt with D at the first position and see whether it outputs d *at any position*. See Figure 10 and Appendix D for details.

**Results.** Table 2 summarizes the results. Both ARM and MDM achieve near-perfect accuracy on the forward mapping across all sequence lengths. On the reverse task, however, the ARMs collapse completely, producing zero correct outputs. In contrast, the MDM achieves substantial success (33–55% depending on  $L$ ), despite never being trained on reversed pairs. This indicates that MDMs can infer the reverse mapping, while ARMs cannot, consistent with the reversal curse observed in large-scale datasets (Section 3).

### 5.1. Attention Correlation

We next verify whether the attention score correlation predicted by Theorem 4.1 is observed in practice. Using the trained one-layer RADD model, we measure attention scores from the [M] token to its paired uppercase token under both forward contexts (“[M] is  $B$ ”) and reverse contexts (“ $B$  is [M]), evaluating across all positional permutations. Intuitively, if forward training increases attention from [M] to  $B$ , our theory predicts a corresponding increase under the reverse context even though that configuration is never seen during training.

As shown in Figure 3, the results confirm this prediction: forward and reverse attention scores are consistently positively correlated across sequence lengths. Even though the forward conditional  $p_\theta(x = A | y = B)$  and the reverse conditional  $p_\theta(y = A | x = B)$  are mathematically unrelated under the training objective, the geometry of RoPE ensures that stronger alignment in one direction statistically reinforces

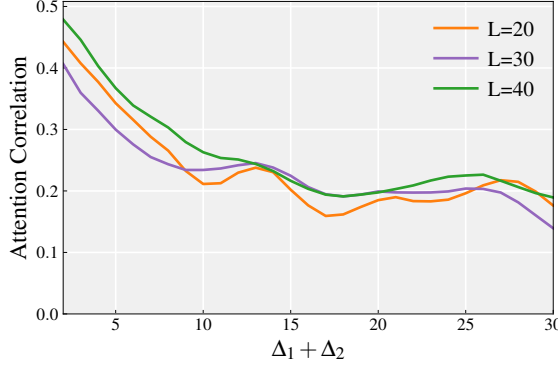


Figure 3. Empirical validation of the attention correlation mechanism. Correlation of attention scores as a function of total relative distance  $\Delta_1 + \Delta_2$  in a one-layer RADD shown for sequence lengths  $L = 20, 30, 40$ . **The consistent positive correlation** provides strong empirical support for Theorem 4.1.

the other. In other words, what we observe empirically is precisely the architectural bias we identified theoretically, operating robustly in trained models.

We further observe that softmaxed attention weights for both directions exhibit highly synchronized growth and convergence throughout training (see Figure 13), with a more comprehensive analysis of these dynamics provided in Appendix E. Such synchronized dynamics provide direct evidence that the encoder’s full-attention mechanism inherently ties the two directions of inference, enabling MDMs to generalize reversal without explicit supervision.

## 5.2. Gradient Alignment

To validate the gradient alignment in Theorem 4.2, we consider a simplified experimental setting. Specifically, we employ an attention-only one-layer Transformer encoder. We also restrict the vocabulary to lowercase–uppercase letter pairs and remove the zero padding, which yields sequence length to  $L = 2$ . This allows us to isolate the training dynamics from effects of context tokens or architectural components.

For a lowercase-uppercase pair, forward and reverse query correspond to  $[\text{M}]\text{D}$  and  $\text{D}[\text{M}]$ , respectively. Gradients are obtained by backpropagating at the  $[\text{M}]$  token and regarding  $\mathbf{g}_{\text{fwd}}$  and  $\mathbf{g}_{\text{rev}}$  as a concatenated vector of all trainable parameters. We use cosine similarity as a proxy for the gradient inner product to clearly quantify the degree of alignment. We measure  $p_\theta(x_i = \text{d} \mid \mathbf{x})$  for tracking probability transfer. Refer to Section D for more details and analyses.

We observe near-perfect gradient alignment between  $\mathbf{g}_{\text{fwd}}$  and  $\mathbf{g}_{\text{rev}}$ , with cosine similarity consistently around 0.999 throughout training. This gradient-level coupling induced by high cosine similarity directly facilitates the probability rise observed in Figure 4. In MDMs, the probability trajectories

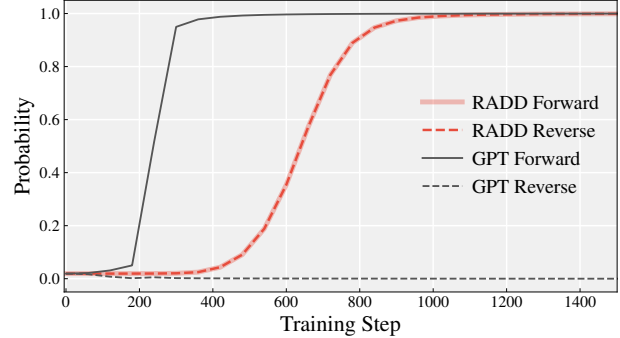


Figure 4. Probability of the ground-truth token under forward and reverse queries. In MDMs, both probabilities increase in tandem, with cosine similarity remaining near 0.999 throughout training.

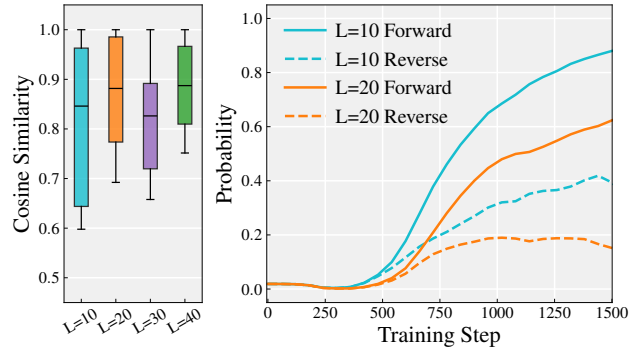


Figure 5. Gradient alignment and probability transfer in one-layer RADD. **Left:** Cosine similarity between forward and reverse gradients during training. **Right:** Probability of the ground-truth token under forward and reverse queries. For all lengths, the cosine similarity remains above 0.6, indicating that the forward and reverse optimization directions remain aligned beyond the minimal setting.

for the forward and reverse directions are nearly identical, rising in tandem until both reach near-perfect recall. However, ARMs fail to assign any significant probability to the target token in the reverse direction. The alignment of gradients and probabilities confirms that updates derived from the forward loss effectively act as a stochastic gradient descent step for the reverse loss, allowing the model to inherently capture the bidirectional relationship.

Beyond the idealized setting, we evaluate whether these dynamics persist in a one-layer Transformer encoder across varying sequence lengths ( $L = 10$  to  $40$ ). As illustrated in Figure 5, the gradient alignment remains robust beyond the idealized setting, forward updates yielding consistently high cosine similarity to the reverse gradients. Consequently, significant probability transfer to the reverse direction also manifests in this setting by showing synchronized patterns of reverse probability rising after the forward. This confirms that the architectural coupling in MDMs ensures forward optimization constructively minimizes the reverse loss even in architectures with MLP and non-linearity.

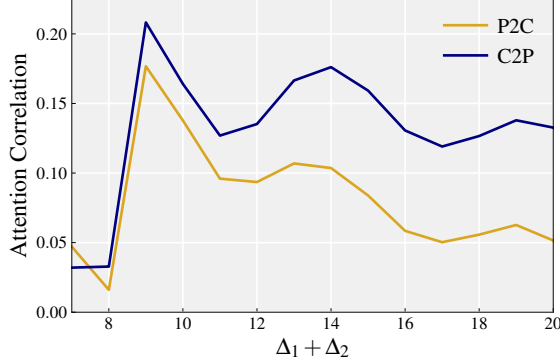


Figure 6. Empirical validation of the Attention Correlation on LLaDA. Analyses reveal stable, positive correlation across relative distances, supporting the proposed coupled learning mechanism.

## 6. Large-Scale Validation

We extend our analysis beyond one-layer Transformer (Section 5) to large-scale Parent-Child dataset evaluating both P2C and C2P. Additional results are shown in Section F.

### 6.1. Attention Correlation

To evaluate attention correlation between forward and reverse contexts we proceed as follows: for every sample and every relative positional permutation we extract the raw attention score (the un-normalized query-key product including RoPE) from the masked position to the position of token  $B$  under the forward context, denoted  $S_{\text{fwd}}$ , and under the reverse context, denoted  $S_{\text{rev}}$ . We then compute the Pearson correlation  $\text{Corr}(S_{\text{fwd}}, S_{\text{rev}})$  across permutations and aggregate these correlations as a function of the total relative distance  $\Delta_{\text{total}} = \Delta_1 + \Delta_2$ .

Figure 6 reports  $\text{Corr}(S_{\text{fwd}}, S_{\text{rev}})$  as a function of the total relative distance  $\Delta_{\text{total}}$  on LLaDA. Consistent with the toy setting, we observe a stable positive correlation across a wide range of relative distances. These results provide large-scale empirical support for our attention-correlation mechanism: even under single-direction supervision, the encoder’s attention geometry induces aligned attention patterns between the forward and reverse contexts.

### 6.2. Gradient Alignment

To measure coupling between forward and reverse objectives, we construct paired masked-prediction queries for each sample and track training dynamics at both the gradient and probabilistic levels. In P2C, we instantiate the forward query from a sample in the Parent-Child dataset (Figure 2), e.g., “[M]’s child is Tom Holland” where [M] denotes a masked entity span. The reverse query flips the direction, e.g., “Tom Holland’s parent is [M]”. For both queries, we compute the negative log-probability of the ground-truth

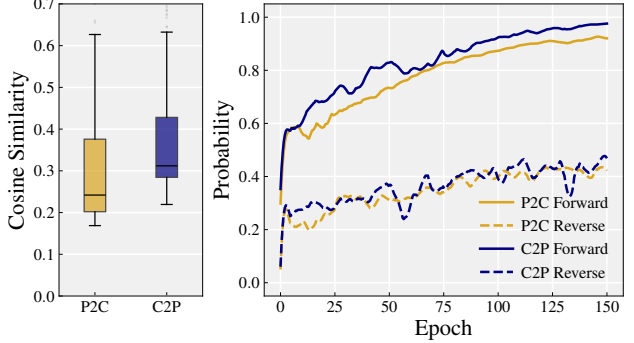


Figure 7. Training dynamics on LLaDA. **Left:** Cosine similarity between forward and reverse gradients remains consistently positive across training, indicating directional alignment. **Right:** Probability of the ground-truth token at the first-unmasked position increases during training for both forward and reverse queries.

token at that position. C2P follows the same procedure with the roles of parent and child swapped.

For each sample and epoch, we compute  $\mathbf{g}_{\text{rev}}$  and  $\mathbf{g}_{\text{fwd}}$  with respect to all trainable parameters and evaluate both their raw inner product and cosine similarity. As shown in Figure 7 (left), the gradient inner product remains positive, and the cosine similarity consistently positive at a meaningful magnitude, indicating directional alignment. These results suggest that parameter updates induced by forward supervision align with those supporting reverse inference.

At the probabilistic level, we record the model-assigned probability of the ground-truth token at the same first-unmasked position. As shown in the right plot of the Figure 7, both forward and reverse probabilities increase steadily over training and exhibit closely matched growth trends. This parallel improvement indicates that gains in forward inference confidence are mirrored by corresponding gains in reverse inference confidence, even though reverse examples are never explicitly trained. Taken together, the gradient- and probability-level analyses indicate that optimization on the forward direction tends to co-improve reverse inference throughout training.

## 7. Conclusion

We analyzed the well-known *reversal curse* in ARMs through the lens of MDMs. In large-scale evaluations, we find that MDMs substantially and consistently alleviate reversal failures that persist in strong ARMs. We further show, both theoretically and empirically, that the training objective alone is insufficient to explain this mitigation, which is instead driven by the interplay between encoder architecture and training dynamics. Our results underscore that understanding and improving MDMs may require analyzing how architectural structure interacts with training dynamics for principled model and sampler design.

## Impact Statement

This paper presents work whose goal is to advance the field of machine learning. There are many potential societal consequences of our work, none of which we feel must be specifically highlighted here.

## References

Abramowitz, M. and Stegun, I. A. *Handbook of mathematical functions: with formulas, graphs, and mathematical tables*, volume 55. Courier Corporation, 1965.

Austin, J., Johnson, D. D., Ho, J., Tarlow, D., and Van Den Berg, R. Structured denoising diffusion models in discrete state-spaces. In *NeurIPS*, 2021.

Berglund, L., Tong, M., Kaufmann, M., Balesni, M., Stickland, A. C., Korbak, T., and Evans, O. The reversal curse: Llms trained on “a is b” fail to learn “b is a”. In *ICLR*, 2024.

Brown, T., Mann, B., Ryder, N., Subbiah, M., Kaplan, J., Dhariwal, P., et al. Language models are few-shot learners. In *NeurIPS*, 2020.

Campbell, A., Benton, J., De Bortoli, V., Rainforth, T., Deligiannidis, G., and Doucet, A. A continuous time framework for discrete denoising models. In *NeurIPS*, 2022.

Cantelli, F. P. Intorno ad un teorema fondamentale della teoria del rischio. *Bollettino dell'Associazione degli Attuari Italiani*, 1910.

Clark, K., Khandelwal, U., Levy, O., and Manning, C. D. What does bert look at? an analysis of bert’s attention. In *ACL Workshop BlackboxNLP*, 2019.

Dasgupta, S. and Gupta, A. An elementary proof of a theorem of johnson and lindenstrauss. *Random Structures & Algorithms*, 2003.

Devlin, J., Chang, M.-W., Lee, K., and Toutanova, K. Bert: Pre-training of deep bidirectional transformers for language understanding. In *NAACL*, 2019.

Elsahar, H., Vougiouklis, P., Remaci, A., Gravier, C., Hare, J., Laforest, F., and Simperl, E. T-REx: A large scale alignment of natural language with knowledge base triples. In *LREC*, 2018.

Golovneva, O., Allen-Zhu, Z., Weston, J. E., and Sukhbaatar, S. Reverse training to nurse the reversal curse. In *COLM*, 2024.

Grattafiori, A., Dubey, A., Jauhri, A., et al. The llama 3 herd of models. *arXiv preprint arXiv:2407.21783*, 2024.

Hu, E. J., yelong shen, Wallis, P., Allen-Zhu, Z., Li, Y., Wang, S., Wang, L., and Chen, W. LoRA: Low-rank adaptation of large language models. In *ICLR*, 2022.

Johnson, W. B., Lindenstrauss, J., et al. Extensions of lipschitz mappings into a hilbert space. *Contemporary mathematics*, 1984.

Kim, J., Shah, K., Kontonis, V., Kakade, S. M., and Chen, S. Train for the worst, plan for the best: Understanding token ordering in masked diffusions. In *ICML*, 2025.

Kitouni, O., Nolte, N., Bouchacourt, D., Williams, A., Rabbat, M., and Ibrahim, M. The factorization curse: Which tokens you predict underlie the reversal curse and more. In *NeurIPS*, 2024.

Lin, Z., Fu, Z., Liu, K., Xie, L., Lin, B., Wang, W., Cai, D., Wu, Y., and Ye, J. Delving into the reversal curse: How far can large language models generalize? In *NeurIPS*, 2024.

Lou, A., Meng, C., and Ermon, S. Discrete diffusion modeling by estimating the ratios of the data distribution. In *ICML*, 2024.

Lu, Z., Jin, L., Li, P., Tian, Y., Zhang, L., Wang, S., Xu, G., Tian, C., and Cai, X. Rethinking the reversal curse of llms: a prescription from human knowledge reversal. In *EMNLP*, 2024.

Lv, A., Zhang, K., Xie, S., Tu, Q., Chen, Y., Wen, J.-R., and Yan, R. An analysis and mitigation of the reversal curse. In *EMNLP*, 2024.

Ng, K. W., Tian, G.-L., and Tang, M.-L. *Dirichlet and related distributions: Theory, methods and applications*. John Wiley & Sons, 2011.

Nie, S., Zhu, F., Du, C., Pang, T., Liu, Q., Zeng, G., Lin, M., and Li, C. Scaling up masked diffusion models on text. In *ICLR*, 2025a.

Nie, S., Zhu, F., You, Z., Zhang, X., Ou, J., Hu, J., ZHOU, J., Lin, Y., Wen, J.-R., and Li, C. Large language diffusion models. In *NeurIPS*, 2025b.

OpenAI. Gpt-4 technical report. *arXiv preprint arXiv:2303.08774*, 2023.

Ou, J., Nie, S., Xue, K., Zhu, F., Sun, J., Li, Z., and Li, C. Your absorbing discrete diffusion secretly models the conditional distributions of clean data. In *ICLR*, 2025.

Radford, A., Narasimhan, K., Salimans, T., and Sutskever, I. Improving language understanding by generative pre-training. *OpenAI Blog*, 2018.

Radford, A., Wu, J., Child, R., Luan, D., Amodei, D., and Sutskever, I. Language models are unsupervised multitask learners. *OpenAI Blog*, 2019.

Raffel, C., Shazeer, N., Roberts, A., Lee, K., Narang, S., Matena, M., Zhou, Y., Li, W., and Liu, P. J. Exploring the limits of transfer learning with a unified text-to-text transformer. *JMLR*, 2020.

Sahoo, S., Arriola, M., Schiff, Y., Gokaslan, A., Marroquin, E., Chiu, J., Rush, A., and Kuleshov, V. Simple and effective masked diffusion language models. In *NeurIPS*, 2024.

Shi, J., Han, K., Wang, Z., Doucet, A., and Titsias, M. Simplified and generalized masked diffusion for discrete data. In *NeurIPS*, 2024.

Su, J., Ahmed, M., Lu, Y., Pan, S., Bo, W., and Liu, Y. Roformer: Enhanced transformer with rotary position embedding. *Neurocomputing*, 2024.

Vaswani, A., Shazeer, N., Parmar, N., Uszkoreit, J., Jones, L., Gomez, A. N., Kaiser, Ł., and Polosukhin, I. Attention is all you need. In *NeurIPS*, 2017.

Yang, A., Yang, B., Zhang, B., Hui, B., Zheng, B., Yu, B., Li, C., Liu, D., Huang, F., Wei, H., Lin, H., Yang, J., Tu, J., Zhang, J., Yang, J., Yang, J., Zhou, J., Lin, J., Dang, K., Lu, K., Bao, K., Yang, K., Yu, L., Li, M., Xue, M., Zhang, P., Zhu, Q., Men, R., Lin, R., Li, T., Tang, T., Xia, T., Ren, X., Ren, X., Fan, Y., Su, Y., Zhang, Y., Wan, Y., Liu, Y., Cui, Z., Zhang, Z., and Qiu, Z. Qwen2.5 technical report. *arXiv preprint arXiv:2412.15115*, 2025.

Ye, J., Xie, Z., Zheng, L., Gao, J., Wu, Z., Jiang, X., Li, Z., and Kong, L. Dream 7b: Diffusion large language models. *arXiv preprint arXiv:2508.15487*, 2025.

Zhang, Y., Bai, R. H., Gu, Z., Zhang, R., Gu, J., Abbe, E., Bengio, S., and Jaity, N. Reversal blessing: Thinking backward may outpace thinking forward in multi-choice questions. *arXiv preprint arXiv:2502.18435*, 2025.

Zhu, H., Huang, B., Zhang, S., Jordan, M., Jiao, J., Tian, Y., and Russell, S. J. Towards a theoretical understanding of the 'reversal curse' via training dynamics. In *NeurIPS*, 2024.

Zucchet, N., Bornschein, J., Chan, S. C., Lampinen, A. K., Pascanu, R., and De, S. How do language models learn facts? dynamics, curricula and hallucinations. In *COLM*, 2025.

## A. Details for Attention Correlation

### A.1. Proof of Theorem 4.1

Let  $\mathbf{q} \in \mathbb{R}^D$  be a random vector with  $\mathbf{q} \sim \mathcal{N}(0, \sigma^2 I)$ , and write  $\mathbf{q} = (\mathbf{q}_1^\top \mathbf{q}_2^\top \cdots \mathbf{q}_m^\top)^\top$ , where  $\mathbf{q}_i \in \mathbb{R}^2$  and  $m = D/2$ . Similarly, decompose  $\mathbf{k} = (\mathbf{k}_1^\top \mathbf{k}_2^\top \cdots \mathbf{k}_m^\top)^\top$  with  $\mathbf{k}_i \in \mathbb{R}^2$ . Assuming that the blocks  $\mathbf{k}_i$  and  $\mathbf{k}_j$  are conditionally independent given  $\mathbf{q}$  for all  $i \neq j$ , the conditional covariance of  $\mathbf{k}$  becomes block diagonal with  $2 \times 2$  blocks:

$$\text{Cov}(\mathbf{k} | \mathbf{q}) = \text{diag}(\Sigma_1(\mathbf{q}), \Sigma_2(\mathbf{q}), \dots, \Sigma_m(\mathbf{q})),$$

where each block  $\Sigma_i(\mathbf{q}) \in \mathbb{R}^{2 \times 2}$  has the same total variance  $\tau^2$  and takes  $\mathbf{q}_i$  as an eigenvector. Let the corresponding eigenvalue be parameterized by  $0 \leq \rho_i(\mathbf{q}) \leq 1$ , so that

$$\Sigma_i(\mathbf{q}) = \tau^2 \left( \frac{1 - \rho_i(\mathbf{q})}{2} I + \rho_i(\mathbf{q}) \frac{\mathbf{q}_i \mathbf{q}_i^\top}{\|\mathbf{q}_i\|^2} \right).$$

The RoPE matrix (Su et al., 2024) is defined to be

$$\mathbf{R}(\Delta) = \text{diag}(R(\Delta\theta_1), \dots, R(\Delta\theta_m)), \quad R(\theta) = \begin{pmatrix} \cos \theta & -\sin \theta \\ \sin \theta & \cos \theta \end{pmatrix}.$$

First, calculate the conditional covariance  $\text{Cov}(\mathbf{q}^\top \mathbf{R}(\Delta) \mathbf{k}, \mathbf{q}^\top \mathbf{R}(-\Delta) \mathbf{k} | \mathbf{q})$ :

$$\begin{aligned} \text{Cov}(\mathbf{q}^\top \mathbf{R}(\Delta) \mathbf{k}, \mathbf{q}^\top \mathbf{R}(-\Delta) \mathbf{k} | \mathbf{q}) &= \text{Cov} \left( \sum_{i=1}^m \mathbf{q}_i^\top R(\Delta\theta_i) \mathbf{k}_i, \sum_{j=1}^m \mathbf{q}_j^\top R(-\Delta\theta_j) \mathbf{k}_j \mid \mathbf{q} \right) \\ &= \sum_{i=1}^m \sum_{j=1}^m \text{Cov}(\mathbf{q}_i^\top R(\Delta\theta_i) \mathbf{k}_i, \mathbf{q}_j^\top R(-\Delta\theta_j) \mathbf{k}_j | \mathbf{q}) \\ &= \sum_{i=1}^m \text{Cov}(\mathbf{q}_i^\top R(\Delta\theta_i) \mathbf{k}_i, \mathbf{q}_i^\top R(-\Delta\theta_i) \mathbf{k}_i | \mathbf{q}) \\ &= \sum_{i=1}^m \mathbf{q}_i^\top R(\Delta\theta_i) \Sigma_i(\mathbf{q}) R(-\Delta\theta_i)^\top \mathbf{q}_i. \end{aligned}$$

The reduction to the diagonal terms uses the conditional independence of  $\mathbf{k}_i$  and  $\mathbf{k}_j$  for  $i \neq j$ . The final equality follows from the standard identity

$$\text{Cov}(\mathbf{a}^\top \mathbf{x}, \mathbf{b}^\top \mathbf{x}) = \mathbf{a}^\top \text{Cov}(\mathbf{x}) \mathbf{b},$$

applied here with  $\mathbf{x} = \mathbf{k}_i$ .

Next, compute the summand  $\mathbf{q}_i^\top R(\Delta\theta_i) \Sigma_i(\mathbf{q}) R(-\Delta\theta_i)^\top \mathbf{q}_i$ :

$$\begin{aligned} \mathbf{q}_i^\top R(\Delta\theta_i) \Sigma_i(\mathbf{q}) R(-\Delta\theta_i)^\top \mathbf{q}_i &= \mathbf{q}_i^\top R(\Delta\theta_i) \tau^2 \left( \frac{1 - \rho_i}{2} I + \frac{\rho_i}{\|\mathbf{q}_i\|^2} \mathbf{q}_i \mathbf{q}_i^\top \right) R(\Delta\theta_i) \mathbf{q}_i \\ &= \tau^2 \left[ \frac{1 - \rho_i}{2} \mathbf{q}_i^\top R(2\Delta\theta_i) \mathbf{q}_i + \frac{\rho_i}{\|\mathbf{q}_i\|^2} (\mathbf{q}_i^\top R(\Delta\theta_i) \mathbf{q}_i)^2 \right] \\ &= \tau^2 \left[ \frac{1 - \rho_i}{2} \|\mathbf{q}_i\|^2 \cos(2\Delta\theta_i) + \frac{\rho_i}{\|\mathbf{q}_i\|^2} (\|\mathbf{q}_i\|^2 \cos(\Delta\theta_i))^2 \right] \\ &= \tau^2 \|\mathbf{q}_i\|^2 \left[ \frac{1}{2} \cos(2\Delta\theta_i) + \rho_i \left( -\frac{1}{2} \cos(2\Delta\theta_i) + \cos^2(\Delta\theta_i) \right) \right] \\ &= \tau^2 \|\mathbf{q}_i\|^2 \left[ \frac{1}{2} \cos(2\Delta\theta_i) + \frac{\rho_i}{2} \right] \\ &= \frac{\tau^2 \|\mathbf{q}_i\|^2}{2} [\cos(2\Delta\theta_i) + \rho_i], \end{aligned}$$

where we used the trigonometric identity

$$\cos(2A) = 2\cos^2(A) - 1.$$

Therefore,

$$\text{Cov}(\mathbf{q}^\top \mathbf{R}(\Delta)\mathbf{k}, \mathbf{q}^\top \mathbf{R}(-\Delta)\mathbf{k} \mid \mathbf{q}) = \frac{\tau^2}{2} \sum_{i=1}^m \|\mathbf{q}_i\|^2 [\cos(2\Delta\theta_i) + \rho_i].$$

The conditional variance is obtained in the same manner:

$$\begin{aligned} \text{Var}(\mathbf{q}^\top \mathbf{R}(\Delta)\mathbf{k} \mid \mathbf{q}) &= \text{Cov}(\mathbf{q}^\top \mathbf{R}(\Delta)\mathbf{k}, \mathbf{q}^\top \mathbf{R}(-\Delta)\mathbf{k} \mid \mathbf{q}) \\ &= \sum_{i=1}^m \mathbf{q}_i^\top R(\Delta\theta_i)\Sigma_i(\mathbf{q})R(\Delta\theta_i)^\top \mathbf{q}_i \\ &= \sum_{i=1}^m \tau^2 \left[ \frac{1 - \rho_i}{2} \mathbf{q}_i^\top \mathbf{q}_i + \frac{\rho_i}{\|\mathbf{q}_i\|^2} (\mathbf{q}_i^\top R(\Delta\theta_i)\mathbf{q}_i)^2 \right] \\ &= \tau^2 \sum_{i=1}^m \|\mathbf{q}_i\|^2 \left[ \frac{1 - \rho_i}{2} + \rho_i \cos^2(\Delta\theta_i) \right] \\ &= \tau^2 \sum_{i=1}^m \|\mathbf{q}_i\|^2 \left[ \frac{1}{2} + \rho_i \left( \cos^2(\Delta\theta_i) - \frac{1}{2} \right) \right] \\ &= \tau^2 \sum_{i=1}^m \|\mathbf{q}_i\|^2 \left[ \frac{1}{2} + \frac{\rho_i}{2} \cos(2\Delta\theta_i) \right] \\ &= \frac{\tau^2}{2} \sum_{i=1}^m \|\mathbf{q}_i\|^2 [1 + \rho_i \cos(2\Delta\theta_i)]. \end{aligned}$$

By the evenness of the cosine function,  $\text{Var}(\mathbf{q}^\top \mathbf{R}(-\Delta)\mathbf{k} \mid \mathbf{q}) = \text{Var}(\mathbf{q}^\top \mathbf{R}(\Delta)\mathbf{k} \mid \mathbf{q})$ . Therefore, the conditional correlation becomes

$$\begin{aligned} \text{Corr}(\mathbf{q}^\top \mathbf{R}(\Delta)\mathbf{k}, \mathbf{q}^\top \mathbf{R}(-\Delta)\mathbf{k} \mid \mathbf{q}) &= \frac{\frac{\tau^2}{2} \sum_{i=1}^m \|\mathbf{q}_i\|^2 [\cos(2\Delta\theta_i) + \rho_i]}{\frac{\tau^2}{2} \sum_{i=1}^m \|\mathbf{q}_i\|^2 [1 + \rho_i \cos(2\Delta\theta_i)]} \\ &= \frac{\sum_{i=1}^m w_i [\cos(2\Delta\theta_i) + \rho_i]}{1 + \sum_{i=1}^m w_i \rho_i \cos(2\Delta\theta_i)}, \end{aligned}$$

where  $w_i = \|\mathbf{q}_i\|^2 / \|\mathbf{q}\|^2$ .

To obtain a lower bound, define

$$A = \sum_{i=1}^m w_i \cos(2\Delta\theta_i), \quad B = \sum_{i=1}^m w_i \rho_i, \quad \text{and} \quad C = \sum_{i=1}^m w_i \rho_i \cos(2\Delta\theta_i).$$

Since

$$A \leq \sum_{i=1}^m w_i |\cos(2\Delta\theta_i)| \leq 1 \quad \text{and} \quad C \leq \sum_{i=1}^m w_i \rho_i |\cos(2\Delta\theta_i)| \leq B,$$

we have  $AC \leq B$ , and therefore  $A(1 + C) = A + AC \leq A + B$ . Thus,

$$\text{Corr}(\mathbf{q}^\top \mathbf{R}(\Delta)\mathbf{k}, \mathbf{q}^\top \mathbf{R}(-\Delta)\mathbf{k} \mid \mathbf{q}) = \frac{A + B}{1 + C} \geq A = \sum_{i=1}^m w_i \cos(2\Delta\theta_i).$$

We now take expectation. Since  $\mathbf{q}_i \stackrel{\text{i.i.d.}}{\sim} \mathcal{N}(0, \sigma^2 I)$ ,

$$\|\mathbf{q}_i\|^2 = q_{2i-1}^2 + q_{2i}^2 \stackrel{\text{i.i.d.}}{\sim} \chi^2(2).$$

By the Gamma–Dirichlet relation (Ng et al., 2011),

$$(w_1, w_2, \dots, w_m) \sim \text{Dirichlet}(1, 1, \dots, 1),$$

which is the uniform distribution over the  $(m - 1)$ -simplex. Hence  $\mathbb{E}[w_i] = 1/m$ , and therefore

$$\mathbb{E}_{\mathbf{q}}[\text{Corr}(\mathbf{q}^\top \mathbf{R}(\Delta) \mathbf{k}, \mathbf{q}^\top \mathbf{R}(-\Delta) \mathbf{k} \mid \mathbf{q})] \geq \sum_{i=1}^m \mathbb{E}[w_i] \cos(2\Delta\theta_i) = \frac{1}{m} \sum_{i=1}^m \cos(2\Delta\theta_i).$$

From the definition of  $\mathbf{R}(\cdot)$ , the last quantity equals  $\frac{1}{D} \text{Tr}(\mathbf{R}(2\Delta))$ .

## A.2. Derivation of the Approximate Inequality (1)

For notational convenience, we write  $\Delta$  in place of  $2\Delta$ . Our objective is to obtain a positive lower bound for

$$\frac{1}{D} \text{Tr}(\mathbf{R}(\Delta)).$$

By the definition of the RoPE matrix,

$$\frac{1}{D} \text{Tr}(\mathbf{R}(\Delta)) = \frac{2}{D} \sum_{s=1}^{D/2} \cos\left(\frac{\Delta}{10000^{\frac{2(s-1)}{D}}}\right).$$

The right-hand side can be recognized as a Riemann sum, since the index  $s$  effectively samples the interval  $[0, 1]$  with step size  $1/(D/2)$ . Therefore,

$$\frac{2}{D} \sum_{s=1}^{\frac{D}{2}} \cos\left(\frac{\Delta}{10000^{\frac{2(s-1)}{D}}}\right) = \int_0^1 \cos\left(\frac{\Delta}{10000^x}\right) dx + O\left(\frac{1}{D}\right).$$

In what follows, we approximate the summation by the integral and study the positivity of the latter. Specifically, we assume

$$\frac{2}{D} \sum_{s=1}^{\frac{D}{2}} \cos\left(\frac{\Delta}{10000^{\frac{2(s-1)}{D}}}\right) \approx \int_0^1 \cos\left(\frac{\Delta}{10000^x}\right) dx,$$

and examine whether the integral is strictly positive. With the change of variables  $u = 10000^{-x}$ , we have  $du = (-\log 10000)u dx$ , and thus

$$\begin{aligned} \int_0^1 \cos\left(\frac{\Delta}{10000^x}\right) dx &= \int_1^{\frac{1}{10000}} \cos(\Delta u) \frac{du}{(-\log 10000)u} \\ &= \frac{1}{\log 10000} \int_{\frac{1}{10000}}^1 \frac{\cos(\Delta u)}{u} du. \end{aligned}$$

This integral can be expressed in terms of the classical cosine integral function  $\text{Ci}(x) = -\int_x^\infty \frac{\cos t}{t} dt$ :

$$\begin{aligned} \int_{\frac{1}{10000}}^1 \frac{\cos(\Delta u)}{u} du &= \int_{\frac{\Delta}{10000}}^{\Delta} \frac{\cos t}{t} dt \\ &= -\int_{\Delta}^{\infty} \frac{\cos t}{t} dt + \int_{\frac{\Delta}{10000}}^{\infty} \frac{\cos t}{t} dt \\ &= \text{Ci}(\Delta) - \text{Ci}\left(\frac{\Delta}{10000}\right). \end{aligned}$$

Combining the above expressions, we obtain

$$\int_0^1 \cos\left(\frac{\Delta}{10000^x}\right) dx = \frac{\text{Ci}(\Delta) - \text{Ci}\left(\frac{\Delta}{10000}\right)}{\log 10000}.$$

We now restrict our attention to the range  $1 \leq \Delta \leq 100$ . To establish positivity, we derive a lower bound on  $\text{Ci}(\Delta)$  and an upper bound on  $\text{Ci}(\Delta/10000)$ .

**Lower bound for  $\text{Ci}(\Delta)$ .** For  $x \geq 1$ , an integration by parts yields

$$\begin{aligned} \text{Ci}(x) &= - \int_x^\infty \frac{\cos t}{t} dt \\ &= \frac{\sin x}{x} - \int_x^\infty \frac{\sin t}{t^2} dt. \end{aligned}$$

Taking absolute values, we obtain

$$\begin{aligned} |\text{Ci}(x)| &\leq \left| \frac{\sin x}{x} \right| + \int_x^\infty \frac{|\sin t|}{t^2} dt \\ &\leq \frac{1}{x} + \int_x^\infty \frac{1}{t^2} dt \\ &= \frac{2}{x}. \end{aligned}$$

Hence,

$$\text{Ci}(x) \geq -\frac{2}{x}.$$

In particular, for  $\Delta \leq 100$ ,

$$\text{Ci}(\Delta) \geq -\frac{2}{\Delta} \geq -\frac{2}{100}.$$

**Upper bound for  $\text{Ci}(\Delta/10000)$ .** It is a classical result that  $\text{Ci}(x)$  admits the alternative representation (Abramowitz & Stegun, 1965):

$$\text{Ci}(x) = \gamma + \log x + \int_0^x \frac{\cos t - 1}{t} dt,$$

where  $\gamma$  is the Euler-Mascheroni constant. Since  $\cos t - 1 \leq 0$ , the integral term is nonpositive, which immediately gives the upper bound

$$\text{Ci}(x) \leq \gamma + \log x.$$

Thus, for  $\Delta \leq 100$ ,

$$\begin{aligned} \text{Ci}\left(\frac{\Delta}{10000}\right) &\leq \gamma + \log\left(\frac{\Delta}{10000}\right) \\ &\leq \gamma + \log\left(\frac{100}{10000}\right) \\ &= \gamma - \log 100. \end{aligned}$$

**Final estimate.** Combining the two bounds, we obtain

$$\begin{aligned} \int_0^1 \cos\left(\frac{\Delta}{10000^x}\right) dx &= \frac{\text{Ci}(\Delta) - \text{Ci}\left(\frac{\Delta}{10000}\right)}{\log 10000} \\ &\geq \frac{-2/100 - \gamma + \log 100}{\log 10000}. \end{aligned}$$

Hence, for  $1 \leq \Delta \leq 100$ , the integral remains strictly positive, which validates our approximation:

$$\frac{1}{D} \text{Tr}(\mathbf{R}(\Delta)) \gtrsim \frac{-2/100 - \gamma + \log 100}{\log 10000} \approx 0.435.$$

In particular, this confirms that the correlation term is bounded away from zero in the regime of interest, ensuring the desired positivity.

### A.3. Derivation of a One-Sided Tail Bound

To derive a Cantelli-type bound for the conditional correlation, we compute the mean and variance of the lower bound  $\sum_{i=1}^m w_i \cos(2\Delta\theta_i)$ . The mean is

$$E := \mathbb{E} \left[ \sum_{i=1}^m w_i \cos(2\Delta\theta_i) \right] = \sum_{i=1}^m \mathbb{E}[w_i] \cos(2\Delta\theta_i) = \frac{1}{m} \sum_{i=1}^m \cos(2\Delta\theta_i),$$

and using  $\mathbb{E}[w_i] = 1/m$  and  $\mathbb{E}[w_i w_j] = (1 + \mathbb{1}[i = j])/(m(m+1))$ , the variance is

$$\begin{aligned} V &:= \text{Var} \left( \sum_{i=1}^m w_i \cos(2\Delta\theta_i) \right) \\ &= \mathbb{E} \left[ \left( \sum_{i=1}^m w_i \cos(2\Delta\theta_i) \right)^2 \right] - \left( \mathbb{E} \left[ \sum_{i=1}^m w_i \cos(2\Delta\theta_i) \right] \right)^2 \\ &= \sum_{i=1}^m \sum_{j=1}^m \cos(2\Delta\theta_i) \cos(2\Delta\theta_j) \mathbb{E}[w_i w_j] - \left( \frac{1}{m} \sum_{i=1}^m \cos(2\Delta\theta_i) \right)^2 \\ &= \sum_{i=1}^m \sum_{j=1}^m \cos(2\Delta\theta_i) \cos(2\Delta\theta_j) \frac{1 + \mathbb{1}[i = j]}{m(m+1)} - \left( \frac{1}{m} \sum_{i=1}^m \cos(2\Delta\theta_i) \right)^2 \\ &= \frac{1}{m(m+1)} \left[ \sum_{i=1}^m \sum_{j=1}^m \cos(2\Delta\theta_i) \cos(2\Delta\theta_j) + \sum_{i=1}^m \cos^2(2\Delta\theta_i) \right] - \frac{1}{m^2} \left( \sum_{i=1}^m \cos(2\Delta\theta_i) \right)^2 \\ &= \frac{1}{m(m+1)} \left[ \left( \sum_{i=1}^m \cos(2\Delta\theta_i) \right)^2 + \sum_{i=1}^m \cos^2(2\Delta\theta_i) \right] - \frac{1}{m^2} \left( \sum_{i=1}^m \cos(2\Delta\theta_i) \right)^2 \\ &= \left( \frac{1}{m(m+1)} - \frac{1}{m^2} \right) \left( \sum_{i=1}^m \cos(2\Delta\theta_i) \right)^2 + \frac{1}{m(m+1)} \sum_{i=1}^m \cos^2(2\Delta\theta_i) \\ &= \frac{m - (m+1)}{m^2(m+1)} \left( \sum_{i=1}^m \cos(2\Delta\theta_i) \right)^2 + \frac{1}{m+1} \left( \frac{1}{m} \sum_{i=1}^m \cos^2(2\Delta\theta_i) \right) \\ &= \frac{-1}{m^2(m+1)} \left( \sum_{i=1}^m \cos(2\Delta\theta_i) \right)^2 + \frac{1}{m+1} \left( \frac{1}{m} \sum_{i=1}^m \cos^2(2\Delta\theta_i) \right) \\ &= \frac{1}{m+1} \left[ \frac{1}{m} \sum_{i=1}^m \cos^2(2\Delta\theta_i) - \left( \frac{1}{m} \sum_{i=1}^m \cos(2\Delta\theta_i) \right)^2 \right]. \end{aligned}$$

Table 3. Lower bounds  $\frac{(E-c)^2}{V+(E-c)^2}$  for  $\Pr[\text{Corr} \geq c]$  under different values of  $\Delta$ ,  $c$  and  $m = D/2$ .

$\Delta$	$c(m = 64)$						$c(m = 128)$					
	0.05	0.10	0.15	0.20	0.25	0.30	0.05	0.10	0.15	0.20	0.25	0.30
10	0.981	0.977	0.972	0.965	0.956	0.941	0.990	0.988	0.986	0.982	0.977	0.970
20	0.967	0.958	0.947	0.930	0.903	0.858	0.985	0.981	0.976	0.969	0.957	0.938
30	0.958	0.947	0.930	0.905	0.863	0.790	0.981	0.976	0.969	0.958	0.939	0.906
40	0.955	0.942	0.923	0.893	0.843	0.752	0.979	0.974	0.965	0.952	0.928	0.885
50	0.965	0.956	0.942	0.921	0.887	0.827	0.979	0.973	0.963	0.949	0.923	0.874

For any threshold  $0 < c \leq E$ , Cantelli's inequality (Cantelli, 1910) gives

$$\begin{aligned} \Pr[\text{Corr}(\mathbf{q}^\top \mathbf{R}(\Delta) \mathbf{k}, \mathbf{q}^\top \mathbf{R}(-\Delta) \mathbf{k} \mid \mathbf{q}) \geq c] &\geq \Pr \left[ \sum_{i=1}^m w_i \cos(2\Delta\theta_i) \geq c \right] \\ &= \Pr \left[ \sum_{i=1}^m w_i \cos(2\Delta\theta_i) - E \geq -(E-c) \right] \\ &\geq \frac{(E-c)^2}{V + (E-c)^2}. \end{aligned}$$

As shown in Table 3, the resulting probability bound  $\frac{(E-c)^2}{V + (E-c)^2}$  can be computed numerically across a range of values of  $\Delta$ ,  $c$  and  $m$ . For instance, with  $\Delta = 20$ ,  $c = 0.3$  and  $m = 128$ , we obtain

$$\Pr[\text{Corr}(\mathbf{q}^\top \mathbf{R}(\Delta) \mathbf{k}, \mathbf{q}^\top \mathbf{R}(-\Delta) \mathbf{k} \mid \mathbf{q}) \geq 0.3] \geq 0.938.$$

## B. Details for Transfer via Gradient Alignment

This appendix provides the detailed derivation underlying Theorem 4.2: (i) a closed-form decomposition of the forward-reverse gradient inner product by parameter block, and (ii) sufficient conditions under which the total inner product is positive.

**Model and simplifications.** We consider a single-layer, single-head Transformer encoder with fixed embeddings, RoPE and trainable parameters  $\mathbf{W}_Q, \mathbf{W}_K, \mathbf{W}_V \in \mathbb{R}^{D \times D}$  and  $\mathbf{W}_O \in \mathbb{R}^{|\mathcal{V}| \times D}$ . We focus on the masked position and isolate the influence of the informative token  $B$  by retaining only the value contribution from  $B$ . Let  $\alpha_{\text{fwd}}$  (resp.  $\alpha_{\text{rev}}$ ) denote the softmaxed attention weight from the  $[\mathbf{M}]$  query to the key of  $B$  in  $\mathbf{x}_{\text{fwd}}$  (resp.  $\mathbf{x}_{\text{rev}}$ ). With  $\mathbf{v}_B = \mathbf{W}_V \mathbf{h}_B$ , the context vectors are

$$\mathbf{c}_{\text{fwd}} = \alpha_{\text{fwd}} \mathbf{v}_B, \quad \mathbf{c}_{\text{rev}} = \alpha_{\text{rev}} \mathbf{v}_B,$$

and the logits are  $\mathbf{z}_{\text{fwd}} = \mathbf{W}_O \mathbf{c}_{\text{fwd}}$  and  $\mathbf{z}_{\text{rev}} = \mathbf{W}_O \mathbf{c}_{\text{rev}}$ , yielding  $p_\theta([\mathbf{M}] = \cdot \mid \mathbf{x}_{\text{fwd}}) = \text{softmax}(\mathbf{z}_{\text{fwd}})$  and  $p_\theta([\mathbf{M}] = \cdot \mid \mathbf{x}_{\text{rev}}) = \text{softmax}(\mathbf{z}_{\text{rev}})$ .

**Errors and backpropagated signals.** Define the probability error vectors

$$\mathbf{e}_{\text{fwd}} = p_\theta([\mathbf{M}] = \cdot \mid \mathbf{x}_{\text{fwd}}) - \mathbb{1}_A, \quad \mathbf{e}_{\text{rev}} = p_\theta([\mathbf{M}] = \cdot \mid \mathbf{x}_{\text{rev}}) - \mathbb{1}_A,$$

and the backpropagated signals at the context vector

$$\mathbf{u}_{\text{fwd}} = \mathbf{W}_O^\top \mathbf{e}_{\text{fwd}}, \quad \mathbf{u}_{\text{rev}} = \mathbf{W}_O^\top \mathbf{e}_{\text{rev}}.$$

Let  $S_{\text{fwd}}$  and  $S_{\text{rev}}$  denote the RoPE attention scores from  $[\mathbf{M}]$  to  $B$ :

$$S_{\text{fwd}} = \mathbf{q}_{[\mathbf{M}]}^\top \mathbf{R}(\Delta_1) \mathbf{k}_B, \quad S_{\text{rev}} = \mathbf{q}_{[\mathbf{M}]}^\top \mathbf{R}(-\Delta_2) \mathbf{k}_B,$$

and write the local softmax derivative factors as

$$\beta_{\text{fwd}} = \alpha_{\text{fwd}}(1 - \alpha_{\text{fwd}}), \quad \beta_{\text{rev}} = \alpha_{\text{rev}}(1 - \alpha_{\text{rev}}).$$

Finally define  $C_t := w_{\mathbf{O},t}^\top \mathbf{v}_B$  and the “margin-like” quantities

$$\mu_{\text{fwd}} = \mathbb{E}_{t \sim p_\theta([\mathbf{M}] = \cdot | \mathbf{x}_{\text{fwd}})}[C_t] - C_A, \quad \mu_{\text{rev}} = \mathbb{E}_{t \sim p_\theta([\mathbf{M}] = \cdot | \mathbf{x}_{\text{rev}})}[C_t] - C_A.$$

**Gradient inner-product decomposition.** For a parameter block  $\mathbf{W} \in \{\mathbf{W}_Q, \mathbf{W}_K, \mathbf{W}_V, \mathbf{W}_O\}$  define

$$I_{\mathbf{W}} := \langle \nabla_{\mathbf{W}} \mathcal{L}_{\text{fwd}}(\theta), \nabla_{\mathbf{W}} \mathcal{L}_{\text{rev}}(\theta) \rangle_F.$$

**Theorem B.1** (Closed-form decomposition). *In the setting above,*

$$\begin{aligned} I_{\mathbf{W}_O} &= \langle \mathbf{e}_{\text{fwd}}, \mathbf{e}_{\text{rev}} \rangle \alpha_{\text{fwd}} \alpha_{\text{rev}} \|\mathbf{v}_B\|^2, \\ I_{\mathbf{W}_V} &= \langle \mathbf{u}_{\text{fwd}}, \mathbf{u}_{\text{rev}} \rangle \alpha_{\text{fwd}} \alpha_{\text{rev}} \|\mathbf{h}_B\|^2, \\ I_{\mathbf{W}_Q} &= \frac{\mu_{\text{fwd}} \mu_{\text{rev}} \beta_{\text{fwd}} \beta_{\text{rev}}}{D} \|\mathbf{h}_{[\mathbf{M}]} \|^2 \mathbf{k}_B^\top \mathbf{R}(\Delta_1 + \Delta_2) \mathbf{k}_B, \\ I_{\mathbf{W}_K} &= \frac{\mu_{\text{fwd}} \mu_{\text{rev}} \beta_{\text{fwd}} \beta_{\text{rev}}}{D} \|\mathbf{h}_B \|^2 \mathbf{q}_{[\mathbf{M}]}^\top \mathbf{R}(\Delta_1 + \Delta_2) \mathbf{q}_{[\mathbf{M}]} \end{aligned}$$

**Corollary B.2** (Positive forward–reverse gradient alignment). *Assume*

- (i) *both contexts are in a non-saturated regime:  $p_\theta(A | \mathbf{x}_{\text{fwd}}) < 1$  and  $p_\theta(A | \mathbf{x}_{\text{rev}}) < 1$ ,*
- (ii) *the backpropagated signals are positively aligned:  $\langle \mathbf{u}_{\text{fwd}}, \mathbf{u}_{\text{rev}} \rangle > 0$ ,*
- (iii) *the scalar gradient magnitudes share the same sign:  $\mu_{\text{fwd}} \mu_{\text{rev}} > 0$ ,*
- (iv) *the RoPE quadratic forms are positive:  $\mathbf{k}_B^\top \mathbf{R}(\Delta_1 + \Delta_2) \mathbf{k}_B > 0$  and  $\mathbf{q}_{[\mathbf{M}]}^\top \mathbf{R}(\Delta_1 + \Delta_2) \mathbf{q}_{[\mathbf{M}]} > 0$ .*

*Then*

$$\langle \mathbf{g}_{\text{rev}}, \mathbf{g}_{\text{fwd}} \rangle = I_{\mathbf{W}_Q} + I_{\mathbf{W}_K} + I_{\mathbf{W}_V} + I_{\mathbf{W}_O} > 0.$$

## B.1. Proof of Theorem B.1

We present the detailed derivation for Theorem B.1. For the sake of brevity, we omit explicit direction indices (fwd, rev) in intermediate steps where the derivation applies symmetrically to both contexts.

**1. Output Projection ( $I_{\mathbf{W}_O}$ ).** We compute the inner product of the gradients with respect to the output projection matrix  $\mathbf{W}_O$ . Recall that the logit for token  $t$  is given by  $z_t = \alpha C_t$ , where  $C_t = w_{\mathbf{O},t}^\top \mathbf{v}_B$  and  $\alpha$  is the scalar attention weight which does not depend on  $\mathbf{W}_O$ .

*Gradient Derivation.* Using the chain rule, the gradient of the loss with respect to  $\mathbf{W}_O$  is:

$$\nabla_{\mathbf{W}_O} \mathcal{L}(\theta) = \sum_{t \in \mathcal{V}} e_t \nabla_{\mathbf{W}_O} z_t = \sum_{t \in \mathcal{V}} e_t (\alpha \nabla_{\mathbf{W}_O} C_t).$$

*Inner Product Expansion.* The inner product between the forward and reverse gradients decomposes as follows:

$$\begin{aligned} I_{\mathbf{W}_O} &= \langle \nabla_{\mathbf{W}_O} \mathcal{L}_{\text{fwd}}(\theta), \nabla_{\mathbf{W}_O} \mathcal{L}_{\text{rev}}(\theta) \rangle_F \\ &= \left\langle \sum_{i \in \mathcal{V}} e_{\text{fwd},i} \alpha_{\text{fwd}} \nabla_{\mathbf{W}_O} C_i, \sum_{j \in \mathcal{V}} e_{\text{rev},j} \alpha_{\text{rev}} \nabla_{\mathbf{W}_O} C_j \right\rangle_F \\ &= \alpha_{\text{fwd}} \alpha_{\text{rev}} \sum_{i \in \mathcal{V}} \sum_{j \in \mathcal{V}} e_{\text{fwd},i} e_{\text{rev},j} \langle \nabla_{\mathbf{W}_O} C_i, \nabla_{\mathbf{W}_O} C_j \rangle_F. \end{aligned}$$

To simplify  $\langle \nabla_{\mathbf{W}_O} C_i, \nabla_{\mathbf{W}_O} C_j \rangle_F$ , we use the following lemma regarding the gradients of the projection rows.

**Lemma B.3.** Let the inner product be the Frobenius inner product  $\langle \mathbf{A}, \mathbf{B} \rangle_F = \text{Tr}(\mathbf{A}^\top \mathbf{B})$ . For  $C_t = w_{\mathbf{O},t}^\top \mathbf{v}_B$ , where  $w_{\mathbf{O},t}$  is the  $t$ -th row of  $\mathbf{W}_{\mathbf{O}}$ :

$$\langle \nabla_{\mathbf{W}_{\mathbf{O}}} C_i, \nabla_{\mathbf{W}_{\mathbf{O}}} C_j \rangle_F = \delta_{ij} \|\mathbf{v}_B\|^2.$$

*Proof.* The gradient of  $C_t$  with respect to the matrix  $\mathbf{W}_{\mathbf{O}}$  is given by the outer product of the one-hot vector  $\mathbf{e}_t$  (corresponding to token  $t$ ) and the value vector  $\mathbf{v}_B$ :

$$\nabla_{\mathbf{W}_{\mathbf{O}}} C_t = \nabla_{\mathbf{W}_{\mathbf{O}}} (w_{\mathbf{O},t}^\top \mathbf{v}_B) = \mathbf{e}_t \mathbf{v}_B^\top.$$

Compute the Frobenius inner product:

$$\begin{aligned} \langle \nabla_{\mathbf{W}_{\mathbf{O}}} C_i, \nabla_{\mathbf{W}_{\mathbf{O}}} C_j \rangle_F &= \text{Tr}((\mathbf{e}_i \mathbf{v}_B^\top)^\top (\mathbf{e}_j \mathbf{v}_B^\top)) \\ &= \text{Tr}(\mathbf{v}_B \mathbf{e}_i^\top \mathbf{e}_j \mathbf{v}_B^\top) \\ &= \text{Tr}((\mathbf{e}_i^\top \mathbf{e}_j)(\mathbf{v}_B^\top \mathbf{v}_B)) \quad (\text{Cyclic property}) \\ &= \delta_{ij} \|\mathbf{v}_B\|^2. \end{aligned}$$

□

*Result for  $I_{\mathbf{W}_{\mathbf{O}}}$ .* Applying Lemma B.3, the double summation collapses to a single summation where  $i = j$ :

$$\begin{aligned} I_{\mathbf{W}_{\mathbf{O}}} &= \alpha_{\text{fwd}} \alpha_{\text{rev}} \sum_{t \in \mathcal{V}} e_{\text{fwd},t} e_{\text{rev},t} \|\mathbf{v}_B\|^2 \\ &= \langle \mathbf{e}_{\text{fwd}}, \mathbf{e}_{\text{rev}} \rangle \alpha_{\text{fwd}} \alpha_{\text{rev}} \|\mathbf{v}_B\|^2. \end{aligned}$$

**2. Value Projection ( $I_{\mathbf{W}_{\mathbf{V}}}$ ).** We now analyze the gradient alignment with respect to the value projection matrix  $\mathbf{W}_{\mathbf{V}}$ . Recall that  $C_t = w_{\mathbf{O},t}^\top \mathbf{v}_B = w_{\mathbf{O},t}^\top \mathbf{W}_{\mathbf{V}} \mathbf{h}_B$ .

*Gradient Derivation.* Using the chain rule, the gradient of the loss with respect to  $\mathbf{W}_{\mathbf{V}}$  involves the outer product of the output weights and the input embedding:

$$\nabla_{\mathbf{W}_{\mathbf{V}}} \mathcal{L}(\theta) = \sum_{t \in \mathcal{V}} e_t \nabla_{\mathbf{W}_{\mathbf{V}}} z_t = \sum_{t \in \mathcal{V}} e_t (\alpha \nabla_{\mathbf{W}_{\mathbf{V}}} C_t).$$

*Inner Product Expansion.* Expanding the inner product of the forward and reverse gradients:

$$\begin{aligned} I_{\mathbf{W}_{\mathbf{V}}} &= \langle \nabla_{\mathbf{W}_{\mathbf{V}}} \mathcal{L}_{\text{fwd}}(\theta), \nabla_{\mathbf{W}_{\mathbf{V}}} \mathcal{L}_{\text{rev}}(\theta) \rangle_F \\ &= \alpha_{\text{fwd}} \alpha_{\text{rev}} \sum_{i \in \mathcal{V}} \sum_{j \in \mathcal{V}} e_{\text{fwd},i} e_{\text{rev},j} \langle \nabla_{\mathbf{W}_{\mathbf{V}}} C_i, \nabla_{\mathbf{W}_{\mathbf{V}}} C_j \rangle_F. \end{aligned}$$

We calculate the inner product of the gradients of linear forms.

**Lemma B.4.** Let  $\mathbf{W} \in \mathbb{R}^{m \times n}$  and  $\mathbf{a}, \mathbf{b} \in \mathbb{R}^m$ ,  $\mathbf{u}, \mathbf{v} \in \mathbb{R}^n$ . Then

$$\nabla_{\mathbf{W}}(\mathbf{a}^\top \mathbf{W} \mathbf{u}) = \mathbf{a} \mathbf{u}^\top, \quad \nabla_{\mathbf{W}}(\mathbf{b}^\top \mathbf{W} \mathbf{v}) = \mathbf{b} \mathbf{v}^\top,$$

and hence

$$\langle \nabla_{\mathbf{W}}(\mathbf{a}^\top \mathbf{W} \mathbf{u}), \nabla_{\mathbf{W}}(\mathbf{b}^\top \mathbf{W} \mathbf{v}) \rangle_F = \langle \mathbf{a} \mathbf{u}^\top, \mathbf{b} \mathbf{v}^\top \rangle_F = (\mathbf{a}^\top \mathbf{b})(\mathbf{u}^\top \mathbf{v}).$$

Applying Lemma B.4 with  $\mathbf{W} = \mathbf{W}_{\mathbf{V}}$ ,  $\mathbf{a} = w_{\mathbf{O},i}$ ,  $\mathbf{b} = w_{\mathbf{O},j}$ , and shared input  $\mathbf{u} = \mathbf{v} = \mathbf{h}_B$ :

$$\langle \nabla_{\mathbf{W}_{\mathbf{V}}} C_i, \nabla_{\mathbf{W}_{\mathbf{V}}} C_j \rangle_F = \langle w_{\mathbf{O},i}, w_{\mathbf{O},j} \rangle \langle \mathbf{h}_B, \mathbf{h}_B \rangle = (w_{\mathbf{O},i}^\top w_{\mathbf{O},j}) \|\mathbf{h}_B\|^2.$$

*Result for  $I_{\mathbf{W}_{\mathbf{V}}}$ .* Substituting this back into the expansion and grouping terms:

$$\begin{aligned} I_{\mathbf{W}_{\mathbf{V}}} &= \alpha_{\text{fwd}} \alpha_{\text{rev}} \|\mathbf{h}_B\|^2 \sum_{i,j} e_{\text{fwd},i} e_{\text{rev},j} (w_{\mathbf{O},i}^\top w_{\mathbf{O},j}) \\ &= \alpha_{\text{fwd}} \alpha_{\text{rev}} \|\mathbf{h}_B\|^2 \left\langle \sum_i e_{\text{fwd},i} w_{\mathbf{O},i}, \sum_j e_{\text{rev},j} w_{\mathbf{O},j} \right\rangle. \end{aligned}$$

Recall the definition of the backpropagated signal  $\mathbf{u} = \mathbf{W}_\mathbf{O}^\top \mathbf{e} = \sum_t e_t w_{\mathbf{O},t}$ . Thus:

$$I_{\mathbf{W}_\mathbf{V}} = \langle \mathbf{u}_{\text{fwd}}, \mathbf{u}_{\text{rev}} \rangle \alpha_{\text{fwd}} \alpha_{\text{rev}} \|\mathbf{h}_B\|^2.$$

**3. Query Projection ( $I_{\mathbf{W}_\mathbf{Q}}$ ).** We analyze the gradient alignment with respect to the query projection matrix  $\mathbf{W}_\mathbf{Q}$ . This involves the chain rule through the attention weight  $\alpha$ .

*Gradient Derivation.* Recall that  $\alpha = \text{softmax}(S_B/\sqrt{D})$ . Let  $\beta = \alpha(1 - \alpha)$  be the derivative of the softmax output w.r.t. the logit  $S_B/\sqrt{D}$ . The gradient of the loss is:

$$\nabla_{\mathbf{W}_\mathbf{Q}} \mathcal{L}(\theta) = \sum_{t \in \mathcal{V}} e_t \nabla_{\mathbf{W}_\mathbf{Q}} (\alpha C_t) = \sum_{t \in \mathcal{V}} e_t C_t \left( \frac{\partial \alpha}{\partial S_B} \nabla_{\mathbf{W}_\mathbf{Q}} S_B \right) = \left( \sum_{t \in \mathcal{V}} e_t C_t \right) \left( \beta \frac{1}{\sqrt{D}} \nabla_{\mathbf{W}_\mathbf{Q}} S_B \right).$$

We define the “margin-like” scalar  $\mu$  as:

$$\mu := \sum_{t \in \mathcal{V}} e_t C_t = \sum_{t \in \mathcal{V}} (p_t - \mathbb{1}_{t=A}) C_t = \mathbb{E}_{t \sim p}[C_t] - C_A.$$

Substituting  $\mu$ , the gradient simplifies to:

$$\nabla_{\mathbf{W}_\mathbf{Q}} \mathcal{L}(\theta) = \frac{\mu \beta}{\sqrt{D}} \nabla_{\mathbf{W}_\mathbf{Q}} S_B.$$

*Inner Product Expansion.*

$$\begin{aligned} I_{\mathbf{W}_\mathbf{Q}} &= \langle \nabla_{\mathbf{W}_\mathbf{Q}} \mathcal{L}_{\text{fwd}}(\theta), \nabla_{\mathbf{W}_\mathbf{Q}} \mathcal{L}_{\text{rev}}(\theta) \rangle_F \\ &= \left\langle \frac{\mu_{\text{fwd}} \beta_{\text{fwd}}}{\sqrt{D}} \nabla_{\mathbf{W}_\mathbf{Q}} S_{\text{fwd},B}, \frac{\mu_{\text{rev}} \beta_{\text{rev}}}{\sqrt{D}} \nabla_{\mathbf{W}_\mathbf{Q}} S_{\text{rev},B} \right\rangle_F \\ &= \frac{\mu_{\text{fwd}} \mu_{\text{rev}} \beta_{\text{fwd}} \beta_{\text{rev}}}{D} \langle \nabla_{\mathbf{W}_\mathbf{Q}} S_{\text{fwd},B}, \nabla_{\mathbf{W}_\mathbf{Q}} S_{\text{rev},B} \rangle_F. \end{aligned}$$

We compute the inner product of the score gradients involving RoPE.

**Lemma B.5.**

$$\langle \nabla_{\mathbf{W}_\mathbf{Q}} S_{\text{fwd},B}, \nabla_{\mathbf{W}_\mathbf{Q}} S_{\text{rev},B} \rangle_F = \|\mathbf{h}_{[\mathbf{M}]}^\top \mathbf{R}(\Delta_1 + \Delta_2) \mathbf{k}_B\|^2.$$

*Proof.* The score is  $S_B = \mathbf{q}_{[\mathbf{M}]}^\top \mathbf{R}(\Delta) \mathbf{k}_B = \mathbf{h}_{[\mathbf{M}]}^\top \mathbf{W}_\mathbf{Q}^\top \mathbf{R}(\Delta) \mathbf{k}_B$ . Using the identity  $\nabla_{\mathbf{W}}(\mathbf{a}^\top \mathbf{W}^\top \mathbf{b}) = \mathbf{b} \mathbf{a}^\top$ , we have  $\nabla_{\mathbf{W}_\mathbf{Q}} S_B = (\mathbf{R}(\Delta) \mathbf{k}_B) \mathbf{h}_{[\mathbf{M}]}^\top$ .

Substituting this into the inner product:

$$\begin{aligned} \langle \nabla_{\mathbf{W}_\mathbf{Q}} S_{\text{fwd},B}, \nabla_{\mathbf{W}_\mathbf{Q}} S_{\text{rev},B} \rangle_F &= \text{Tr} \left( \left( \mathbf{R}(\Delta_1) \mathbf{k}_B \mathbf{h}_{[\mathbf{M}]}^\top \right)^\top \left( \mathbf{R}(-\Delta_2) \mathbf{k}_B \mathbf{h}_{[\mathbf{M}]}^\top \right) \right) \\ &= \text{Tr} \left( \mathbf{h}_{[\mathbf{M}]} \mathbf{k}_B^\top \mathbf{R}(\Delta_1)^\top \mathbf{R}(-\Delta_2) \mathbf{k}_B \mathbf{h}_{[\mathbf{M}]}^\top \right) \\ &= \text{Tr}(\mathbf{h}_{[\mathbf{M}]}^\top \mathbf{h}_{[\mathbf{M}]}) \text{Tr}(\mathbf{k}_B^\top \mathbf{R}(-\Delta_1) \mathbf{R}(-\Delta_2) \mathbf{k}_B). \end{aligned}$$

Using the rotation property  $\mathbf{R}(\theta_1) \mathbf{R}(\theta_2) = \mathbf{R}(\theta_1 + \theta_2)$ , we get  $\mathbf{R}(-\Delta_1 - \Delta_2)$ . Since the quadratic form  $\mathbf{x}^\top \mathbf{R}(\theta) \mathbf{x} = \|\mathbf{x}\|^2 \cos \theta$  is an even function of  $\theta$ , we have  $\mathbf{k}_B^\top \mathbf{R}(-(\Delta_1 + \Delta_2)) \mathbf{k}_B = \mathbf{k}_B^\top \mathbf{R}(\Delta_1 + \Delta_2) \mathbf{k}_B$ . Thus,

$$\langle \nabla_{\mathbf{W}_\mathbf{Q}} S_{\text{fwd},B}, \nabla_{\mathbf{W}_\mathbf{Q}} S_{\text{rev},B} \rangle_F = \|\mathbf{h}_{[\mathbf{M}]}^\top \mathbf{R}(\Delta_1 + \Delta_2) \mathbf{k}_B\|^2.$$

□

*Result for  $I_{\mathbf{W}_\mathbf{Q}}$ .* Combining the scalar factors and the lemma:

$$I_{\mathbf{W}_\mathbf{Q}} = \frac{\mu_{\text{fwd}} \mu_{\text{rev}} \beta_{\text{fwd}} \beta_{\text{rev}}}{D} \|\mathbf{h}_{[\mathbf{M}]}^\top \mathbf{R}(\Delta_1 + \Delta_2) \mathbf{k}_B\|^2.$$

**4. Key Projection ( $I_{\mathbf{W}_K}$ ).** We analyze the gradient alignment with respect to the key projection matrix  $\mathbf{W}_K$ . This mirrors the derivation for  $\mathbf{W}_Q$  but involves the gradient of the key vector  $\mathbf{k}_B = \mathbf{W}_K \mathbf{h}_B$ .

*Gradient Derivation.* Using the chain rule through the attention weight  $\alpha$  and defining  $\beta = \alpha(1 - \alpha)$  and  $\mu = \sum_{t \in \mathcal{V}} e_t C_t$ :

$$\nabla_{\mathbf{W}_K} \mathcal{L}(\theta) = \sum_{t \in \mathcal{V}} e_t C_t \nabla_{\mathbf{W}_K} \alpha = \mu \left( \frac{\partial \alpha}{\partial S_B} \nabla_{\mathbf{W}_K} S_B \right) = \frac{\mu \beta}{\sqrt{D}} \nabla_{\mathbf{W}_K} S_B.$$

*Inner Product Expansion.* Expanding the inner product for the forward and reverse gradients:

$$\begin{aligned} I_{\mathbf{W}_K} &= \langle \nabla_{\mathbf{W}_K} \mathcal{L}_{\text{fwd}}(\theta), \nabla_{\mathbf{W}_K} \mathcal{L}_{\text{rev}}(\theta) \rangle_F \\ &= \frac{\mu_{\text{fwd}} \mu_{\text{rev}} \beta_{\text{fwd}} \beta_{\text{rev}}}{D} \langle \nabla_{\mathbf{W}_K} S_{\text{fwd}, B}, \nabla_{\mathbf{W}_K} S_{\text{rev}, B} \rangle_F. \end{aligned}$$

We compute the inner product of the score gradients with respect to  $\mathbf{W}_K$ .

**Lemma B.6.** *Let  $\mathbf{q} = \mathbf{q}_{[\mathbf{M}]}$ . Then:*

$$\langle \nabla_{\mathbf{W}_K} S_{\text{fwd}, B}, \nabla_{\mathbf{W}_K} S_{\text{rev}, B} \rangle_F = \|\mathbf{h}_B\|^2 (\mathbf{q}^\top \mathbf{R}(\Delta_1 + \Delta_2) \mathbf{q}).$$

*Proof.* The attention score is  $S_B = \mathbf{q}^\top \mathbf{R}(\Delta) \mathbf{k}_B = \mathbf{q}^\top \mathbf{R}(\Delta) \mathbf{W}_K \mathbf{h}_B$ . Using the identity  $(\mathbf{AB})^\top = \mathbf{B}^\top \mathbf{A}^\top$ , we can rewrite this as a linear form in  $\mathbf{W}_K$ :

$$S_B = (\mathbf{R}(\Delta)^\top \mathbf{q})^\top \mathbf{W}_K \mathbf{h}_B = (\mathbf{R}(-\Delta) \mathbf{q})^\top \mathbf{W}_K \mathbf{h}_B.$$

Using the gradient identity  $\nabla_{\mathbf{W}}(\mathbf{a}^\top \mathbf{W} \mathbf{b}) = \mathbf{a} \mathbf{b}^\top$ , we have:

$$\nabla_{\mathbf{W}_K} S_B = (\mathbf{R}(-\Delta) \mathbf{q}) \mathbf{h}_B^\top.$$

Now, compute the inner product for the forward case ( $\Delta = \Delta_1$ ) and reverse case ( $\Delta = -\Delta_2$ ):

$$\begin{aligned} \langle \nabla_{\mathbf{W}_K} S_{\text{fwd}, B}, \nabla_{\mathbf{W}_K} S_{\text{rev}, B} \rangle_F &= \text{Tr} \left( ((\mathbf{R}(-\Delta_1) \mathbf{q}) \mathbf{h}_B^\top)^\top ((\mathbf{R}(\Delta_2) \mathbf{q}) \mathbf{h}_B^\top) \right) \\ &= \text{Tr} (\mathbf{h}_B \mathbf{q}^\top \mathbf{R}(-\Delta_1)^\top \mathbf{R}(\Delta_2) \mathbf{q} \mathbf{h}_B^\top) \\ &= \text{Tr} (\mathbf{h}_B \mathbf{h}_B^\top) \text{Tr} (\mathbf{q}^\top \mathbf{R}(\Delta_1) \mathbf{R}(\Delta_2) \mathbf{q}) \\ &= \|\mathbf{h}_B\|^2 (\mathbf{q}^\top \mathbf{R}(\Delta_1 + \Delta_2) \mathbf{q}). \end{aligned}$$

□

*Result for  $I_{\mathbf{W}_K}$ .* Combining the scalar factors and the lemma:

$$I_{\mathbf{W}_K} = \frac{\mu_{\text{fwd}} \mu_{\text{rev}} \beta_{\text{fwd}} \beta_{\text{rev}}}{D} \|\mathbf{h}_B\|^2 \left( \mathbf{q}_{[\mathbf{M}]}^\top \mathbf{R}(\Delta_1 + \Delta_2) \mathbf{q}_{[\mathbf{M}]} \right).$$

## B.2. Proof of Corollary B.2

Given the decomposition in Theorem B.1, the total gradient inner product is the sum of the components derived above. We determine the sign of each term analytically under the assumptions:

**Output Projection ( $I_{\mathbf{W}_O}$ ).** The term is given by  $I_{\mathbf{W}_O} = \langle \mathbf{e}_{\text{fwd}}, \mathbf{e}_{\text{rev}} \rangle \alpha_{\text{fwd}} \alpha_{\text{rev}} \|\mathbf{v}_B\|^2$ . The error vector is  $\mathbf{e} = \mathbf{p} - \mathbb{1}_A$ . Decomposing the inner product at the target index  $A$  and non-target indices  $t \neq A$ :

$$\langle \mathbf{e}_{\text{fwd}}, \mathbf{e}_{\text{rev}} \rangle = (p_{\text{fwd}, A} - 1)(p_{\text{rev}, A} - 1) + \sum_{t \neq A} p_{\text{fwd}, t} p_{\text{rev}, t}.$$

Since  $p < 1$ , the first term is the product of two negative numbers, yielding a large positive value that dominates the sum. The second term is strictly positive as probabilities are non-negative. Thus,  $\langle \mathbf{e}_{\text{fwd}}, \mathbf{e}_{\text{rev}} \rangle > 0$ , implying  $I_{\mathbf{W}_O} > 0$ .

**Value Projection ( $I_{W_V}$ ).** The term is  $I_{W_V} = \langle \mathbf{u}_{\text{fwd}}, \mathbf{u}_{\text{rev}} \rangle \alpha_{\text{fwd}} \alpha_{\text{rev}} \|\mathbf{h}_B\|^2$ . By Assumption (ii), the backpropagated signals are positively aligned, i.e.,  $\langle \mathbf{u}_{\text{fwd}}, \mathbf{u}_{\text{rev}} \rangle > 0$ . Since attention weights  $\alpha \in (0, 1)$  and norms are positive, it follows directly that  $I_{W_V} > 0$ .

**Query and Key Projections ( $I_{W_Q}, I_{W_K}$ ).** These terms are  $I_{W_Q} \propto \mathbf{k}_B^\top \mathbf{R}(\Delta_{\text{sum}}) \mathbf{k}_B$  and  $I_{W_K} \propto \mathbf{q}_{[M]}^\top \mathbf{R}(\Delta_{\text{sum}}) \mathbf{q}_{[M]}$ , sharing the scalar coefficient:

$$C = \frac{\mu_{\text{fwd}} \mu_{\text{rev}} \beta_{\text{fwd}} \beta_{\text{rev}}}{D}.$$

We verify the sign of  $C$  and the geometric factors: 1.  $\beta = \alpha(1 - \alpha) > 0$  for  $\alpha \in (0, 1)$ . 2. By Assumption (iii), margins are consistent:  $\mu_{\text{fwd}} \mu_{\text{rev}} > 0$ . Hence,  $C > 0$ . 3. By Assumption (iv), the RoPE quadratic forms are positive:  $\mathbf{k}_B^\top \mathbf{R}(\Delta_1 + \Delta_2) \mathbf{k}_B > 0$ . Therefore, both products are strictly positive:  $I_{W_Q} > 0$  and  $I_{W_K} > 0$ .

**Conclusion.** Summing these strictly positive terms, we obtain  $\langle \mathbf{g}_{\text{rev}}, \mathbf{g}_{\text{fwd}} \rangle > 0$ .

### B.3. Theoretical and Empirical Justification for Assumptions in Corollary B.2

The validity of the four assumptions in Corollary B.2, which are required for the forward gradient to constructively decrease the reverse loss, is grounded in the following theoretical and empirical observations:

**Assumption (i): Non-saturation Regime** ( $p_\theta([M] = A | x) < 1$ ). This assumption posits that the model is in an active learning phase. Although it may seem technically trivial, it is a fundamental prerequisite for the existence of a transfer signal. If the model were to achieve perfect confidence ( $p_\theta([M] = A | x_{\text{fwd}}) = 1$ ), the error vector would vanish ( $\mathbf{e}_{\text{fwd}} = \mathbf{p} - \mathbb{1}_A = \mathbf{0}$ ). Since every gradient component derived in Theorem B.1 ( $\nabla_{W_O} \mathcal{L}$ ,  $\nabla_{W_V} \mathcal{L}$ ,  $\nabla_{W_Q} \mathcal{L}$ , and  $\nabla_{W_K} \mathcal{L}$ ) is proportional to  $\mathbf{e}_{\text{fwd}}$  (either directly or via the margin scalar  $\mu_{\text{fwd}}$ ), the total forward gradient would identically become zero ( $\nabla_\theta \mathcal{L}_{\text{fwd}} = \mathbf{0}$ ). In such a saturated state, no parameter update occurs ( $\Delta\theta = 0$ ), rendering the mechanism of “transfer via gradient step” undefined. In practice, however, the asymptotic nature of the softmax function ensures that the probability never reaches exactly 1 with finite logits, thereby guaranteeing that this condition holds throughout any non-trivial training phase.

**Assumption (ii): Positive Alignment of Backpropagated Signals** ( $\langle \mathbf{u}_{\text{fwd}}, \mathbf{u}_{\text{rev}} \rangle > 0$ ). We justify this assumption by decomposing the alignment into two stages: first, establishing positive correlation in the probability error space, and second, showing that this correlation is preserved when backpropagated through the output projection matrix  $\mathbf{W}_O$ , even in the presence of training dynamics.

First, we establish that the error vectors  $\mathbf{e}_{\text{fwd}}$  and  $\mathbf{e}_{\text{rev}}$  are positively aligned solely due to the structure of the cross-entropy task.

**Lemma B.7** (Cross-Entropy Error Alignment). *Let  $\mathbf{p}, \mathbf{q} \in \Delta^{|\mathcal{V}|}$  be two probability distributions and  $\mathbb{1}_A$  be the one-hot target vector for token  $A$ . Define error vectors  $\mathbf{e}(\mathbf{p}) = \mathbf{p} - \mathbb{1}_A$  and  $\mathbf{e}(\mathbf{q}) = \mathbf{q} - \mathbb{1}_A$ . Under Assumption (i) (non-saturation,  $p_A < 1, q_A < 1$ ), the inner product is strictly positive:*

$$\langle \mathbf{e}(\mathbf{p}), \mathbf{e}(\mathbf{q}) \rangle \geq (1 - p_A)(1 - q_A) > 0.$$

*Proof.* Expanding the inner product:

$$\begin{aligned} \langle \mathbf{e}(\mathbf{p}), \mathbf{e}(\mathbf{q}) \rangle &= \langle \mathbf{p} - \mathbb{1}_A, \mathbf{q} - \mathbb{1}_A \rangle \\ &= \sum_{t \in \mathcal{V}} p_t q_t - p_A - q_A + 1. \end{aligned}$$

Since  $p_t, q_t \geq 0$ , we have the inequality  $\sum_t p_t q_t \geq p_A q_A$ . Substituting this yields:

$$\langle \mathbf{e}(\mathbf{p}), \mathbf{e}(\mathbf{q}) \rangle \geq p_A q_A - p_A - q_A + 1 = (1 - p_A)(1 - q_A).$$

Furthermore, considering the norms, the cosine similarity is bounded away from zero (specifically  $\cos \angle(\mathbf{e}(\mathbf{p}), \mathbf{e}(\mathbf{q})) \geq 1/2$ ) for typical probability configurations where the target probability is not negligible.  $\square$

We now show that the positive alignment established in the error space is preserved when mapped to the hidden space via  $\mathbf{u} = \mathbf{W}_O^\top \mathbf{e}$ . We model the output matrix as a perturbation of a random initialization:  $\mathbf{W}_O = \mathbf{P}_0 + \Delta$ . Here,  $\mathbf{P}_0$  represents the initial weight matrix with isotropic Gaussian entries, and  $\Delta$  denotes the parameter drift accumulated during training. Intuitively,  $\mathbf{P}_0$  acts as an approximate isometry akin to the Johnson-Lindenstrauss lemma (Johnson et al., 1984; Dasgupta & Gupta, 2003), preserving the acute angle between error vectors with high probability. The following lemma formalizes that this geometric property is robust to training dynamics: provided the spectral norm of the drift  $\Delta$  does not exceed a certain threshold, the forward and reverse gradients remain positively aligned.

**Proposition B.8** (Positive Alignment of Backpropagated Signals). *Let  $\mathbf{P}_0 \in \mathbb{R}^{D \times |\mathcal{V}|}$  be a random matrix with i.i.d. entries drawn from  $\mathcal{N}(0, 1/D)$ . Let the trained matrix be  $\mathbf{P} = \mathbf{P}_0 + \Delta$ , where the perturbation satisfies  $\|\Delta\|_2 \leq \delta$ . Consider two unit vectors  $\mathbf{a}, \mathbf{b} \in \mathbb{R}^{|\mathcal{V}|}$  such that their cosine similarity is  $\langle \mathbf{a}, \mathbf{b} \rangle \geq 1/2$ .*

*Then, with probability at least  $1 - 3 \exp(-\frac{D}{128})$  over the initialization  $\mathbf{P}_0$ , the inner product after projection remains strictly positive:*

$$\langle \mathbf{P}\mathbf{a}, \mathbf{P}\mathbf{b} \rangle > 0,$$

*provided the spectral drift  $\delta$  is sufficiently small (specifically,  $\delta \leq 1/32$  is a sufficient condition).*

*Proof.* Let  $\mathbf{u}(\mathbf{a}) = (\mathbf{P}_0 + \Delta)\mathbf{a}$  and  $\mathbf{u}(\mathbf{b}) = (\mathbf{P}_0 + \Delta)\mathbf{b}$ . We decompose the inner product into a signal term determined by the initialization and noise terms induced by the drift:

$$\begin{aligned} \langle \mathbf{u}(\mathbf{a}), \mathbf{u}(\mathbf{b}) \rangle &= \langle \mathbf{P}_0\mathbf{a} + \Delta\mathbf{a}, \mathbf{P}_0\mathbf{b} + \Delta\mathbf{b} \rangle \\ &= \underbrace{\langle \mathbf{P}_0\mathbf{a}, \mathbf{P}_0\mathbf{b} \rangle}_{\text{Signal}} + \underbrace{\langle \mathbf{P}_0\mathbf{a}, \Delta\mathbf{b} \rangle}_{\text{Cross Terms}} + \underbrace{\langle \Delta\mathbf{a}, \mathbf{P}_0\mathbf{b} \rangle}_{\text{Cross Terms}} + \underbrace{\langle \Delta\mathbf{a}, \Delta\mathbf{b} \rangle}_{\text{Quadratic Noise}}. \end{aligned}$$

We analyze the probabilistic bounds for the signal and the deterministic bounds for the noise separately.

First, consider the Signal term. Since  $\mathbf{a}$  and  $\mathbf{b}$  are fixed unit vectors and  $\mathbf{P}_0$  has i.i.d.  $\mathcal{N}(0, 1/D)$  entries, the projections  $\mathbf{P}_0\mathbf{a}$  and  $\mathbf{P}_0\mathbf{b}$  are random vectors in  $\mathbb{R}^D$  with mean zero and covariance  $\mathbf{I}_D/D$ . The inner product  $\langle \mathbf{P}_0\mathbf{a}, \mathbf{P}_0\mathbf{b} \rangle$  is an unbiased estimator of  $\langle \mathbf{a}, \mathbf{b} \rangle$ . By standard concentration inequalities for random projections (a variant of the Johnson-Lindenstrauss lemma (Johnson et al., 1984; Dasgupta & Gupta, 2003)), the probability that the inner product deviates from its expectation by more than  $\epsilon$  decays exponentially with  $D$ :

$$\Pr(\langle \mathbf{P}_0\mathbf{a}, \mathbf{P}_0\mathbf{b} \rangle < \langle \mathbf{a}, \mathbf{b} \rangle - \epsilon) \leq \exp\left(-\frac{D\epsilon^2}{8}\right).$$

Similarly, the squared norms concentrate around 1. For the upper bound,  $\Pr(\|\mathbf{P}_0\mathbf{a}\|^2 > 1 + \epsilon) \leq \exp(-D\epsilon^2/8)$ . We choose a margin of  $\epsilon = 1/4$ . Applying the union bound to the lower tail of the inner product and the upper tails of the norms of  $\mathbf{a}$  and  $\mathbf{b}$ , with probability at least  $1 - 3 \exp\left(-\frac{D(1/4)^2}{8}\right) = 1 - 3 \exp\left(-\frac{D}{128}\right)$ , the following inequalities hold simultaneously:

$$\langle \mathbf{P}_0\mathbf{a}, \mathbf{P}_0\mathbf{b} \rangle \geq \frac{1}{2} - \frac{1}{4} = \frac{1}{4}, \quad \text{and} \quad \|\mathbf{P}_0\mathbf{a}\| \leq \sqrt{1 + \frac{1}{4}} \approx 1.12 < 1.25.$$

Next, we bound the Noise terms using the spectral norm condition  $\|\Delta\|_2 \leq \delta$  and the Cauchy-Schwarz inequality. Using the concentrated bound  $\|\mathbf{P}_0\mathbf{a}\| \leq 1.25$ :

$$\begin{aligned} |\text{Cross Terms}| &\leq \|\mathbf{P}_0\mathbf{a}\| \|\Delta\mathbf{b}\| + \|\Delta\mathbf{a}\| \|\mathbf{P}_0\mathbf{b}\| \\ &\leq (1.25)(\delta \|\mathbf{b}\|) + (\delta \|\mathbf{a}\|)(1.25) \\ &= 2.5\delta. \quad (\text{since } \|\mathbf{a}\| = \|\mathbf{b}\| = 1) \end{aligned}$$

The quadratic noise is bounded by  $\|\Delta\mathbf{a}\| \|\Delta\mathbf{b}\| \leq \delta^2$ .

Finally, combining the lower bound on the signal and the upper bound on the noise magnitude:

$$\langle \mathbf{u}(\mathbf{a}), \mathbf{u}(\mathbf{b}) \rangle \geq \frac{1}{4} - 2.5\delta - \delta^2.$$

We substitute the condition  $\delta = 1/32 = 0.03125$  to verify positivity:

$$\frac{1}{4} - 2.5(0.03125) - (0.03125)^2 \approx 0.25 - 0.078 - 0.001 = 0.171 > 0.$$

Thus, provided  $\delta \leq 1/32$ , the total inner product remains strictly positive with high probability. Applying this to the normalized error vectors confirms the assumption.  $\square$

**Assumption (iii): Sign Consistency of Margins** ( $\mu_{\text{fwd}}\mu_{\text{rev}} > 0$ ). We show that as training progresses,  $\mu$  consistently becomes negative.

The quantity  $\mu$  is defined as:

$$\mu = \sum_{t \in \mathcal{V}} e_t C_t = \mathbb{E}_{t \sim p(\cdot | \mathbf{x})}[C_t] - C_A,$$

where  $C_t = w_{\mathbf{O},t}^\top \mathbf{v}_B$  is the logit component for token  $t$  given context token  $B$ .  $\mu$  measures the “margin” between the model’s expected predicted logit and the actual target logit.

**Lemma B.9** (Sign Consistency of Margins). *Let  $C_A$  be the target logit component. If the model assigns the highest score to the target token (i.e.,  $C_A \geq C_t$  for all  $t \in \mathcal{V}$ ), then the margin is non-positive:*

$$\mu = \mathbb{E}_{t \sim p}[C_t] - C_A \leq 0.$$

Furthermore, if  $C_A$  is the strict maximum and the model is not saturated ( $p_A < 1$ ), then  $\mu < 0$ . Consequently, satisfying this condition for both contexts implies  $\mu_{\text{fwd}}\mu_{\text{rev}} > 0$ .

*Proof.* The term  $\mathbb{E}_{t \sim p}[C_t]$  is a convex combination of scores bounded above by their maximum. Since  $\max_t C_t = C_A$  by assumption, it immediately follows that  $\mathbb{E}[C_t] \leq C_A$ . The strictly negative case holds because the probability mass is distributed among tokens with strictly lower scores ( $C_t < C_A$ ).  $\square$

We analyze how a single SGD step on the forward objective reinforces this condition.

**Proposition B.10** (Margin Enhancement via Forward SGD). *A single SGD step updating the output projection matrix  $\mathbf{W}_\mathbf{O}$  on the forward context  $\mathbf{x}_{\text{fwd}}$  monotonically increases the margin between the target logit component  $C_A$  and any non-target component  $C_{t \neq A}$ .*

*Proof.* The gradient of the forward loss with respect to  $\mathbf{W}_\mathbf{O}$  is given by  $\nabla_{\mathbf{W}_\mathbf{O}} \mathcal{L}_{\text{fwd}} = \mathbf{e}_{\text{fwd}} \mathbf{c}_{\text{fwd}}^\top$ . Using a learning rate  $\eta > 0$  and the relation  $\mathbf{c}_{\text{fwd}} = \alpha_{\text{fwd}} \mathbf{v}_B$ , the SGD update rule for the  $t$ -th row  $w_{\mathbf{O},t}$  is:

$$w_{\mathbf{O},t}^+ = w_{\mathbf{O},t} - \eta \mathbf{e}_{\text{fwd},t} (\alpha_{\text{fwd}} \mathbf{v}_B).$$

The change in the logit component  $C_t = w_{\mathbf{O},t}^\top \mathbf{v}_B$  is derived as:

$$\begin{aligned} \Delta C_t &= (w_{\mathbf{O},t}^+)^{\top} \mathbf{v}_B - w_{\mathbf{O},t}^\top \mathbf{v}_B \\ &= -\eta \mathbf{e}_{\text{fwd},t} \alpha_{\text{fwd}} \mathbf{v}_B^\top \mathbf{v}_B \\ &= -\eta \alpha_{\text{fwd}} \|\mathbf{v}_B\|^2 \mathbf{e}_{\text{fwd},t}. \end{aligned}$$

Since  $\eta$ ,  $\alpha_{\text{fwd}}$ , and  $\|\mathbf{v}_B\|^2$  are strictly positive, the sign of  $\Delta C_t$  is determined solely by the negative of the error term  $\mathbf{e}_{\text{fwd},t} = p_{\text{fwd},t} - \mathbb{1}_{t=A}$ :

- **Target Token ( $t = A$ ):** Since  $p_{\text{fwd},A} < 1$ , the error is negative ( $\mathbf{e}_{\text{fwd},A} < 0$ ), implying  $\Delta C_A > 0$ .
- **Incorrect Token ( $t \neq A$ ):** Since  $p_{\text{fwd},t} > 0$ , the error is positive ( $\mathbf{e}_{\text{fwd},t} > 0$ ), implying  $\Delta C_t < 0$ .

Consequently, the target score increases while incorrect scores decrease, strictly increasing the margin  $C_A - C_{t \neq A}$ . This validates Assumption (iii) that  $\mu \leq 0$  holds as training proceeds.  $\square$

**Assumption (iv): Positivity of RoPE Quadratic Forms.** This assumption signifies that the geometric alignment induced by RoPE remains constructive even when combining the relative distances of the forward and reverse directions.

The RoPE rotation matrix  $\mathbf{R}(\Delta)$  induces a quadratic form that is an even function of the displacement  $\Delta$ , meaning it is independent of the sign (direction) of the relative distance.

**Lemma B.11** (Evenness of RoPE Quadratic Form). *Let the RoPE matrix be  $\mathbf{R}(\Delta) = \text{diag}(\mathbf{R}(\Delta\theta_1), \dots, \mathbf{R}(\Delta\theta_{D/2}))$ . For any vector  $\mathbf{x} \in \mathbb{R}^D$ , let it be decomposed into  $D/2$  blocks  $\mathbf{x}^{(s)} = (x_{2s-1}, x_{2s})^\top \in \mathbb{R}^2$  for  $s = 1, \dots, D/2$ . Then:*

$$\mathbf{x}^\top \mathbf{R}(\Delta) \mathbf{x} = \sum_{s=1}^{D/2} \cos(\Delta\theta_s) \|\mathbf{x}^{(s)}\|^2.$$

Consequently,  $\mathbf{x}^\top \mathbf{R}(-\Delta) \mathbf{x} = \mathbf{x}^\top \mathbf{R}(\Delta) \mathbf{x}$ .

*Proof.* The total quadratic form is the sum of the quadratic forms for each diagonal block. Expanding the term for the  $s$ -th block:

$$\begin{aligned} (\mathbf{x}^{(s)})^\top \mathbf{R}(\Delta\theta_s) \mathbf{x}^{(s)} &= (x_{2s-1} \ x_{2s}) \begin{pmatrix} \cos \Delta\theta_s & -\sin \Delta\theta_s \\ \sin \Delta\theta_s & \cos \Delta\theta_s \end{pmatrix} \begin{pmatrix} x_{2s-1} \\ x_{2s} \end{pmatrix} \\ &= (x_{2s-1}^2 + x_{2s}^2) \cos \Delta\theta_s \\ &= \|\mathbf{x}^{(s)}\|^2 \cos(\Delta\theta_s). \end{aligned}$$

Summing this over all  $s = 1, \dots, D/2$  yields the result. Since  $\cos(\phi) = \cos(-\phi)$ , the quadratic form is invariant to the sign of  $\Delta$ .  $\square$

The RoPE rotation matrix  $\mathbf{R}(\Delta)$  induces a quadratic form whose sign depends on the geometric alignment of the embedding space.

**Proposition B.12** (Positivity of the RoPE Quadratic Form). *Assume the key vector  $\mathbf{k}$  is drawn from an isotropic distribution  $\mathbf{k} \sim \mathcal{N}(\mathbf{0}, \sigma^2 \mathbf{I})$ . For typical sequence lengths  $\Delta \leq 100$ , the expected normalized quadratic form has a strictly positive lower bound:*

$$\mathbb{E}_{\mathbf{k}} \left[ \frac{\mathbf{k}^\top \mathbf{R}(\Delta) \mathbf{k}}{\|\mathbf{k}\|^2} \right] \approx \frac{1}{D} \text{Tr}(\mathbf{R}(\Delta)) \gtrsim 0.435.$$

*Proof.* The detailed derivation of this bound, which utilizes an integral approximation involving the Cosine Integral function, is provided in Section A.2.  $\square$

The same logic applies symmetrically to the query vector  $\mathbf{q}_{[\mathbf{M}]}$ . Since the quadratic form is defined by the same matrix  $\mathbf{R}(\Delta)$ , assuming  $\mathbf{q}_{[\mathbf{M}]}$  also follows an approximately isotropic distribution (common at initialization), the term  $\mathbf{q}_{[\mathbf{M}]}^\top \mathbf{R}(\Delta) \mathbf{q}_{[\mathbf{M}]}$  satisfies the same positivity condition. Thus, both geometric factors in the gradient decomposition contribute positively.

## C. Details on Large-Scale Experiment

### C.1. Experimental Setup

**Datasets.** We evaluated on three benchmarks adapted from Berglund et al. (2024) and Elsahar et al. (2018): (i) **Parent–Child**, which contains 250 child–parent pairs annotated with parent type (father/mother), (ii) **Person–Description**, which contains 10 entities, each paired with 30 unique name-free descriptions, and (iii) **T-REx**, which contains 90 entities with 6 relations, each paired with 5 unique name-free descriptions. For all datasets, training uses only forward mappings (e.g., Parent→Child or Person→Description), while evaluation is conducted on both forward and reverse directions. Exact-match accuracy is reported after minimal normalization (lowercasing, whitespace stripping). In Parent–Child, either father or mother is accepted as correct when both apply.

#### Parent–Child (P2C)

```
"prompt": "Craig Hemsworth's child is"
"completion": "Chris Hemsworth"
```

**Child–Parent (C2P).**

```
"prompt": "Chris Hemsworth's parent is"
"completion": "Craig Hemsworth"
```

**Person–Description (P2D).**

```
"prompt": "Daphne Barrington, known far and wide for being"
"completion": "the acclaimed director of the virtual reality masterpiece, A
Journey Through Time."
```

**Description–Person (D2P).**

```
"prompt": "The renowned composer of the world's first underwater
symphony, Abyssal Melodies, is called"
"completion": "Uriah Hawthorne"
```

**T-REx.**

```
"prompt": "Helvane has its largest and most important capital city in"
"completion": "State of Orlith"
```

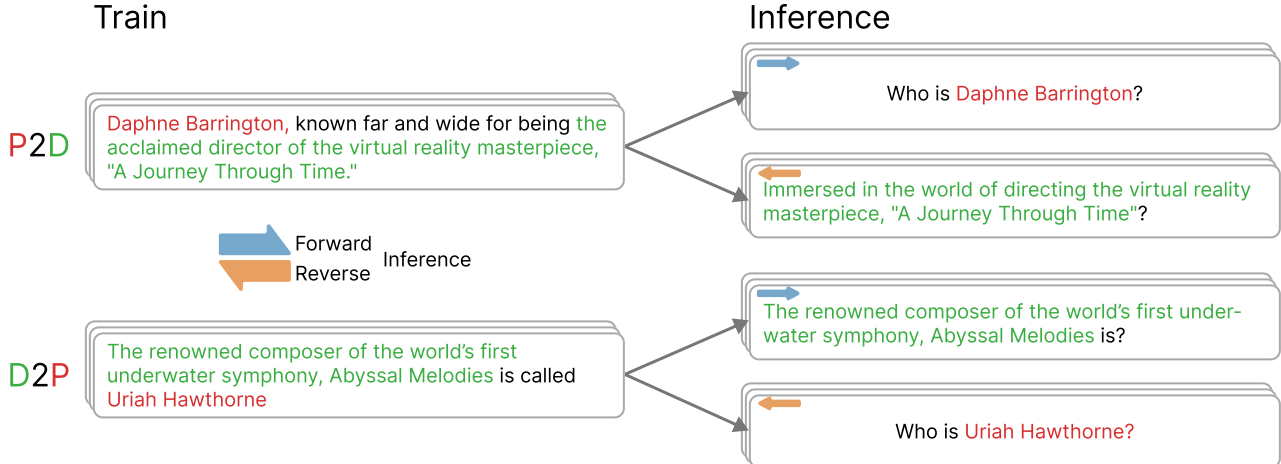


**Figure 8.** Illustration of large-scale experiments on the Person-Description dataset. Each dataset is trained in one direction (e.g., person→description or description→person) and evaluated in both forward and reverse regimes. Forward queries follow the trained mapping, while reverse queries swap input and target roles. The figure shows representative examples of the evaluation setup used to measure exact-match accuracy.

**Training Details** All models were fine-tuned using LoRA adapters with rank  $r = 32$  and scaling  $\alpha = 64$ , applied to attention projection matrices. We used the AdamW optimizer with weight decay 0.1, batch size 8, and trained for 150 epochs. Each experiment was repeated with three random seeds (1, 42, 1234). Evaluation used greedy decoding with temperature  $T = 0$  and maximum generation length 32.

- **LLaDA (Masked Diffusion Model)**

Model: GSAI-ML/LLaDA-8B-Instruct.

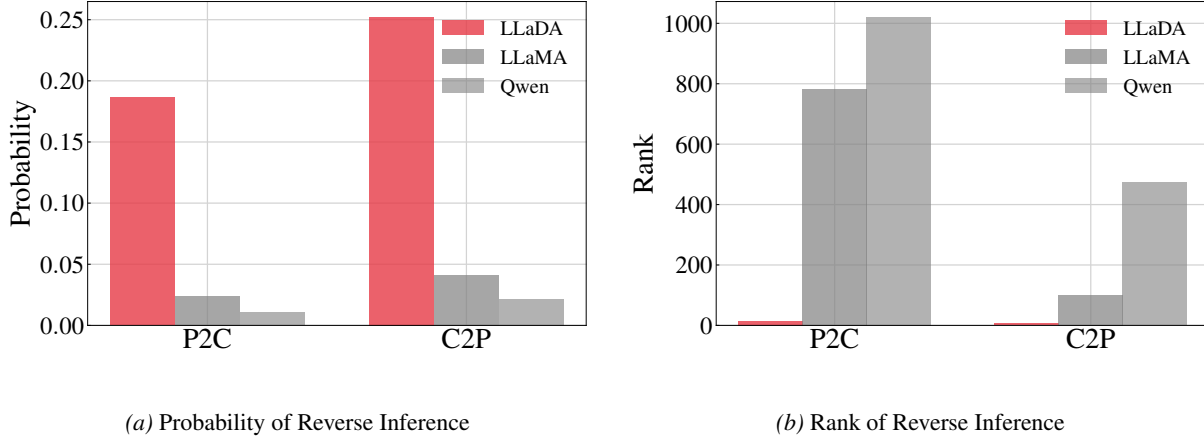


Figure 9. Probability and rank analysis for reverse inference at large-scale using the Parent-Child dataset. (a) Model-assigned probability of the ground-truth token. MDM (LLaDA) consistently assigns higher probability than ARMs. (b) Rank of the correct token (lower is better). MDM ranks the correct reverse token near the top across examples.

Learning rate:  $5 \times 10^{-5}$ ,  $2 \times 10^{-4}$  (for T-REx).

Training used forward diffusion steps of size 32 and block size 32.

- **LLaMA-3.1 (Autoregressive Model)**

Model: `meta-llama/Meta-Llama-3.1-8B-Instruct`.

Learning rate:  $5 \times 10^{-5}$ ,  $9 \times 10^{-5}$  (for T-REx).

The tokenizer pad token was set to EOS, with right-side padding.

- **Qwen-2.5 (Autoregressive Model)**

Model: `Qwen/Qwen2.5-7B-Instruct`.

Learning rate:  $1 \times 10^{-4}$  (slightly higher than LLaDA and LLaMA for stability),  $5 \times 10^{-5}$  (for T-REx).

Tokenizer setup followed the official implementation.

In all settings, exact-match accuracy was computed after normalization (lowercasing and whitespace stripping). Checkpoints were saved every 10 epochs, and the best forward and reverse accuracies were logged using Weights & Biases.

## C.2. Results

Tables 4, 5 and 6 report seed-level accuracies. Across all seeds, ARMs (LLaMA-3.1, Qwen-2.5) reach high accuracy in the forward direction ( $\approx 90\text{--}100\%$ ), but collapse in reverse ( $\leq 16\%$  in Parent-Child and  $\leq 4\%$  in Person-Description). By contrast, LLaDA (MDM) maintains robust reverse performance:  $\approx 44\text{--}48\%$  in Parent-Child reverse tasks and nearly 100% in Person-Description reverse tasks. These seed-level results confirm that the reversal advantage of MDMs is consistent and not an artifact of random initialization.

Table 4. Parent-Child raw results across seeds. F = Forward, R = Reverse.

Seed	Parent $\rightarrow$ Child						Child $\rightarrow$ Parent					
	LLaDA		LLaMA		Qwen		LLaDA		LLaMA		Qwen	
	F	R	F	R	F	R	F	R	F	R	F	R
1	84	45	88	19	90	0	86	48	91.0	6.0	91.0	1.0
42	74	41	91	13	84	0	92	38	100.0	7.1	88.1	2.3
1234	72	59	90.6	15.6	95.8	1.6	85	45	96.8	7.6	88.0	1.0
Avg.	76.7	48.3	89.9	15.9	89.9	0.5	87.7	43.7	95.9	6.9	89.0	1.4

Table 5. Person–Description raw results across seeds. F = Forward, R = Reverse.

Seed	Person→Description						Description→Person					
	LLaDA		LLaMA		Qwen		LLaDA		LLaMA		Qwen	
	F	R	F	R	F	R	F	R	F	R	F	R
1	72.5	100.0	73.0	2.0	73.0	0.5	100	47.5	78.0	1.5	80.5	1.0
42	69.5	99.5	74.0	2.5	69.5	4.0	99	40.5	90.5	0.5	86.0	2.5
1234	76.0	99.0	71.0	6.0	69.5	2.0	100	36.0	80.5	3.5	73.5	1.0
Avg.	72.7	99.5	72.7	3.5	70.7	2.2	99.7	41.3	83.0	1.8	80.0	1.5

Table 6. T-REx raw results across seeds. F = Forward, R = Reverse.

Seed	LLaDA		LLaMA		Qwen	
	F	R	F	R	F	R
1	91.5	80.0	91.0	2.5	99.5	2.5
42	92.5	87.0	92.5	2.5	88.5	2.5
1234	93.0	77.5	78.5	3.5	81.5	2.0
Avg.	92.3	81.5	87.3	2.8	89.8	2.3

## D. Details on Toy Experiments

### D.1. Toy Experiment Data Construction

To isolate the reversal capability, we construct a controlled synthetic dataset using case-pairs. For a sequence length  $L$ , we generate all possible permutations where the lowercase token  $A$  appears at index  $i$  and the uppercase token  $B$  appears at index  $j$ , such that  $i < j$  (forward ordering). All other positions are padded with zeros.

For example, consider a sequence length  $L = 3$  and the pair (d, D). The valid training instances are:

- dD0 (indices 0, 1)
- d0D (indices 0, 2)
- 0dD (indices 1, 2)

Conversely, reversed forms such as Dd0, D0d, and 0Dd (where  $i > j$ ) are strictly excluded from the training set. This ensures that the model never observes the reverse dependency  $B \rightarrow A$  during optimization. At test time, we prompt the model with the uppercase token (e.g., D) to evaluate if it can recover the lowercase counterpart (e.g., d) which is never observed during training.

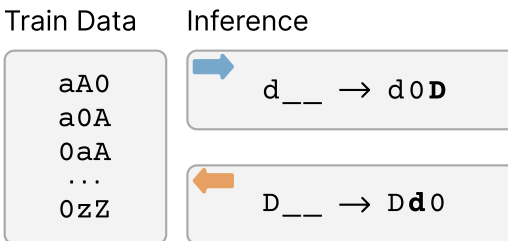


Figure 10. Models are trained on sequences of the form “A is B”. Forward inference uses lowercase prompts, while reverse inference uses uppercase prompts unseen during training.

## D.2. Hyperparameters

The toy experiments for both the one-layer RADD and GPT-2 models were conducted using the hyperparameters detailed in Table 7. All models were trained for a total of 3,000 steps. In addition to the common parameters, the RADD model utilized an exponential moving average (EMA) with a decay rate of 0.9999.

Table 7. Hyperparameters for toy experiments.

Hyperparameter	Value
Batch Size	256
Learning Rate	$3 \times 10^{-4}$
Gradient Clipping	1.0
Weight Decay	0.0
Dropout	0.02
Learning Rate Warmup Steps	1,000
Hidden Dimension	256
Number of Attention Heads	1

## D.3. Sampling Strategy in Toy Experiments

In our large-scale experiments, the LLaDA model employs a confidence based sampling strategy where the next token to unmask is selected based on confidence scores (Kim et al., 2025). For the controlled toy experiments, however, we adopted a simpler method to ensure a fair comparison between the MDM and ARM. We utilized top- $k$  sampling with  $k=3$  for all generations. In this approach, the model restricts its choice to the  $k$  most probable tokens from its output distribution and then samples from this reduced set.

The implementation of top- $k$  sampling differs slightly based on the model architecture. For the ARM (GPT-2), given a prompt, the model computes a probability distribution for the next token in the sequence. It then samples from the top  $k$  candidates to continue the generation. For the MDM (RADD), the process is applied to the masked position. The model computes a probability distribution over the vocabulary for the [M] token and samples from the top  $k$  choices to fill that position. This consistent sampling strategy allows for a direct and fair evaluation of each model’s capabilities on the toy tasks.

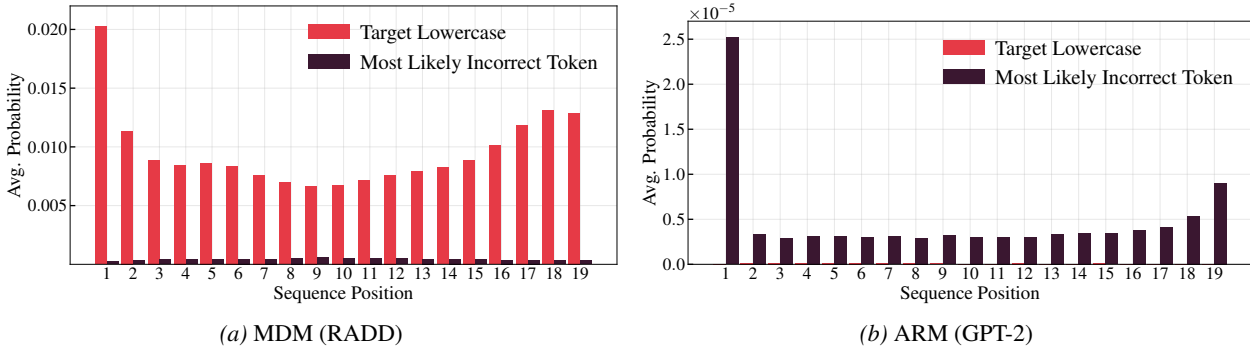


Figure 11. Reverse inference on the toy dataset ( $L = 20$ ). At each position we display the model’s probability for the target lowercase corresponding to the given uppercase (Red), and the maximum probability over all other vocabulary characters (Black). RADD (MDM) consistently assigns higher probability to the correct lowercase, whereas GPT-2 (ARM) fails to allocate meaningful probability to target characters, revealing an architectural gap.

## D.4. Comparative Analysis of Probability Distributions and Gradient Alignment

This section provides a comparative evaluation of the probability mass allocated to ground-truth versus incorrect tokens during reverse inference, alongside the full results for gradient alignment and probability transfer across varying sequence lengths.

To measure the probability, success rate. : Table 2, Figure 11 permutation : Figure 4, Figure 5, Figure 12

To measure probability mass allocation in Figure 11, we evaluate the model’s confidence in generating the target token  $\text{d}$  at each valid generation slot. Specifically, given the masked prompt  $\mathbf{x} = [\text{D}, [\text{M}], \dots, [\text{M}]]$ , we compute the marginal probability  $p_\theta(x_i = \text{d} \mid \mathbf{x})$  for every masked index  $i$ . Since ARMs do not utilize mask tokens, given the prompt  $\mathbf{x} = [\text{D}]$ , we measure the  $p_\theta(x_i = \text{d} \mid \mathbf{x}_{<i})$  for every generation index  $i$ . Also, we compare the correct token versus most likely incorrect token (incorrect token with highest probability except the padding token).

For probability in Figure 4 and Figure 12, we adopt permutation based measuring. For  $i > j$ , the reverse mapping of length  $L$  prompt  $\mathbf{x}$  is expressed as:

$$x_{\text{pos}} = \begin{cases} \text{D} & \text{pos} = j \\ [\text{M}] & \text{pos} = i \\ 0 & \text{otherwise.} \end{cases}$$

Then we measure  $p_\theta(x_i = \text{d} \mid \mathbf{x})$  for MDMs. However, since it is impossible to inject  $[\text{M}]$  due to its autoregressive nature in ARMs, we simply crop the prompt  $\mathbf{x}_{<i}$  and measure  $p_\theta(x_i = \text{d} \mid \mathbf{x}_{<i})$  at position  $i$ . Since we consider all possible sequences that can be generated in permutation-based setting, measuring at position  $i$  and averaging over whole possible cases removes position bias. For examples of permutation-based analysis, refer to Section E

As shown in Figure 11, for a sequence length of  $L = 20$ , the MDM consistently assigns significantly higher probability mass to the correct lowercase target (e.g., predicting  $\text{d}$  when prompted with  $\text{D}$ ) than to the most likely incorrect vocabulary character. In contrast, the ARM (GPT-2) fails to allocate meaningful probability to the target characters, assigning virtually zero mass to the correct mapping while consistently favoring incorrect alternatives. This confirms that ARMs perform no better than random guessing in the reverse direction, while MDMs successfully capture the underlying bidirectional association.

Figure 12 presents the complete training dynamics in Section 5.2 for sequence lengths  $L \in \{10, 20, 30, 40\}$ . This figure supplements the Figure 5 visualizing the probability of ground-token for  $L = 30$  and  $L = 40$  and also comparing with ARMs.

## E. Details on Attention Analysis

### E.1. Methodology for Permutation-Based Analysis

This section details the methodology used in analyzing the attention correlation and the attention weight dynamics in Section 5 for each sequence length  $L = 10, 20, 30, 40$ .

To obtain the correlation as a function of  $\Delta_1 + \Delta_2$  and attention weights, we measured across all corresponding pairs of forward and reverse positional permutations. A forward permutation refers to a unique placement of the character pair where the lowercase letter precedes the uppercase one. For instance, in a sequence of length  $L = 4$ , the set of forward permutations and their corresponding relative distances ( $\Delta_1$ ) are:

$$\text{aA00 } (\Delta_1 = 1), \text{a0A0 } (\Delta_1 = 2), \text{a00A } (\Delta_1 = 3), \\ 0\text{aA0 } (\Delta_1 = 1), 0\text{a0A } (\Delta_1 = 2), 00\text{aA } (\Delta_1 = 1),$$

...

$$\text{zZ00 } (\Delta_1 = 1), \text{z0Z0 } (\Delta_1 = 2), \text{z00Z } (\Delta_1 = 3), \\ 0\text{zZ0 } (\Delta_1 = 1), 0\text{z0Z } (\Delta_1 = 2), 00\text{zZ } (\Delta_1 = 1)$$

A reverse permutation is one where the uppercase letter precedes the lowercase one. The corresponding reverse permutations

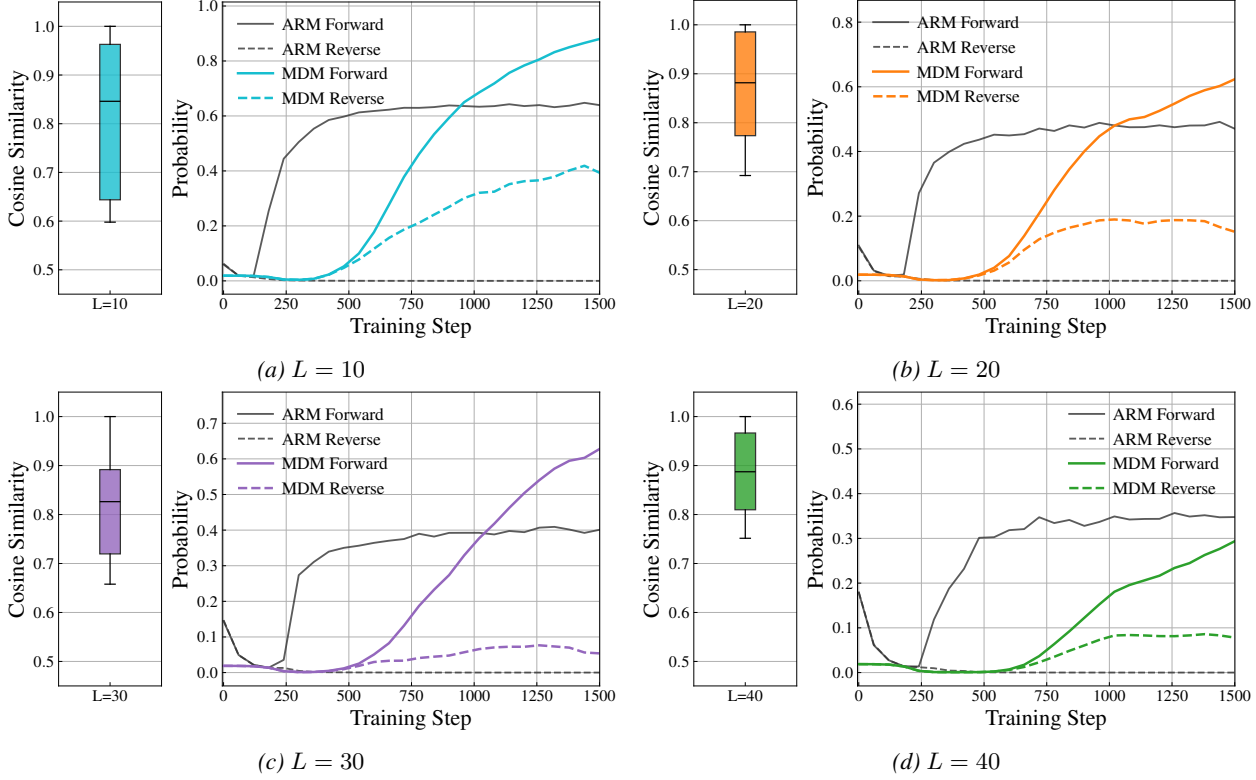


**Figure 12.** Detailed gradient alignment and training dynamics across sequence lengths. Panels (a)–(d) display results for sequence lengths  $L = 10, 20, 30$ , and  $40$ , respectively. In each panel, the box plot (left) illustrates the cosine similarity between forward and reverse gradients, while the line plot (right) tracks the probability of ground-truth token under forward and reverse queries for ARM and MDM methods over training steps. While MDMs assign the probability of the ground-truth token in the reverse mapping, ARMs (grey) assign zero probability.

for the examples above have the same relative distances ( $\Delta_2$ ):

$$\text{Aa00 } (\Delta_2 = 1), \text{A0a0 } (\Delta_2 = 2), \text{A00a } (\Delta_2 = 3),$$

$$\text{0Aa0 } (\Delta_2 = 1), \text{0A0a } (\Delta_2 = 2), \text{00Aa } (\Delta_2 = 1),$$

...

$$\text{Zz00 } (\Delta_2 = 1), \text{Z0z0 } (\Delta_2 = 2), \text{Z00z } (\Delta_2 = 3),$$

$$\text{0Zz0 } (\Delta_2 = 1), \text{0Z0z } (\Delta_2 = 2), \text{00ZZ } (\Delta_2 = 1)$$

For each corresponding pair of forward and reverse permutations with distances  $\Delta_1$  and  $\Delta_2$ , the correlation between their respective attention scores is calculated. To obtain these scores for the analysis, the lowercase character in each permutation is replaced with a [M] token. We then measure the attention the [M] token pays to the uppercase context character (A...Z).

The analysis for both the attention score correlation and the attention weight dynamics follows this identical permutation-based averaging procedure. The only distinction lies in the specific quantity measured: the former uses the raw dot-product attention scores ( $\mathbf{q}^\top R(\Delta)\mathbf{k}$ ), while the latter uses the softmax-normalized attention weights. This approach ensures that our findings reflect the fundamental behavior of the attention mechanism, independent of specific token positions.

## E.2. Further Attention Analysis Results

This section presents the full results of our attention analysis for all tested sequence lengths, complementing the findings discussed in Section 5.

We further analyze by tracking the evolution of attention weights from the [M] token to the uppercase token. For the forward setting, we average the softmaxed weight across all “[M] is B” permutations, and for the reverse setting across all “B

is  $[M]$ ” permutations. The trajectories in Figure 13 reveal a striking pattern: both forward and reverse weights increase together during training, rising sharply at early steps and converging toward similar plateaus. This co-movement indicates that the model does not learn forward and reverse attention in isolation; rather, once the encoder strengthens the forward pathway, the reverse pathway is reinforced as well. Such synchronized dynamics provide direct evidence that the encoder’s full-attention mechanism inherently ties the two directions of inference, enabling MDMs to generalize reversal without explicit supervision.

Figure 13 (left column) shows the empirical correlation of attention scores as a function of total relative distance,  $\Delta_1 + \Delta_2$ , for sequence lengths  $L = 10, 20, 30$ , and  $40$ . The results across all four settings suggest that the correlation between forward and reverse attention scores trends positive, despite considerable variance in the measurements. This consistent positive trend across different sequence lengths suggests that the underlying architectural property is a robust feature of the model, not an artifact of a specific configuration.

Similarly, Figure 13 (right column) visualizes the dynamics of the softmaxed attention weights for both forward and reverse contexts throughout the 3,000 training steps. In all tested sequence lengths, the weights for both contexts demonstrate a strong parallel trajectory, rising sharply and converging together in a coordinated pattern. This co-movement provides strong visual evidence that the model establishes the association of both directions while learning with a unidirectional train data, reinforcing our claim that this behavior is driven by the underlying correlation induced by the full-attention mechanism.

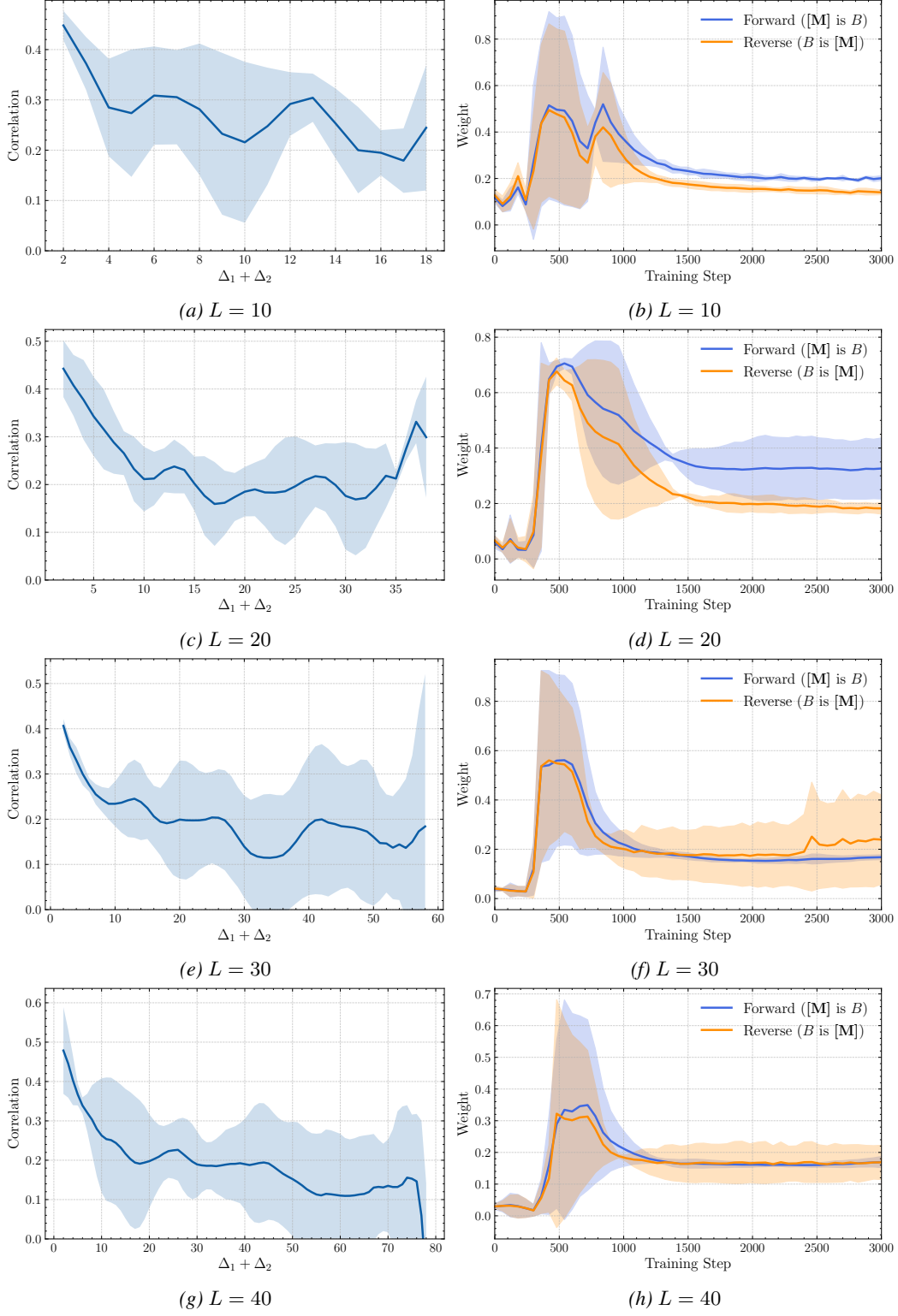


Figure 13. Empirical validation of the attention mechanism's role in reverse inference across various sequence lengths. The left column shows the correlation of attention scores as a function of total relative distance  $\Delta_1 + \Delta_2$ , while the right column shows the dynamics of softmaxed attention weights for forward (blue) and reverse (orange) contexts during training. Each row corresponds to a different  $L = 10, 20, 30, 40$ , respectively. Across all settings, the plots reveal two key findings: (1) a consistent positive correlation between forward and reverse attention scores, and (2) a strong parallel trajectory in the development of attention weights. Taken together, these results provide strong empirical evidence that the full-attention architecture inherently couples forward and reverse contexts, driving the concurrent learning of both directions.

## F. Large-scale Training Dynamics Analysis

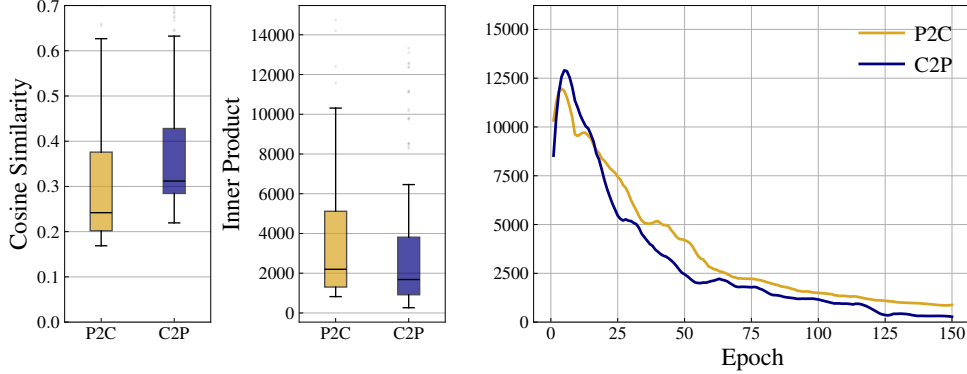


Figure 14. From left to right: (i) box plot of the cosine similarity between the forward and reverse gradients, (ii) box plot of the inner product between the forward and reverse gradients, and (iii) line plot of the inner product between the forward and reverse gradients across training epochs. All three plots consistently exhibit strictly positive values, indicating strong and persistent gradient alignment throughout training. This positivity implies that optimization in the forward direction constructively transfers to the reverse objective. Results are averaged across 3 random seeds.